Systems/Circuits

# Somatic Depolarization Enhances Hippocampal CA1 Dendritic Spike Propagation and Distal Input-Driven Synaptic Plasticity

**Tobias Bock, Adrian Negrean, and Steven A. Siegelbaum**
Departments of Neuroscience and Pharmacology, Vagelos College of Physicians and Surgeons, Kavli Institute for Brain Science, Zuckerman Mind Brain Behavior Institute, Columbia University, New York, New York 10027

**Synaptic inputs that target distal regions of neuronal dendrites can often generate local dendritic spikes that can amplify synaptic depolarization, induce synaptic plasticity, and enhance neuronal output. However, distal dendritic spikes are subject to significant attenuation by dendritic cable properties, and often produce only a weak subthreshold depolarization of the soma. Nonetheless, such spikes have been implicated in memory storage, sensory perception and place field formation. How can such a weak somatic response produce such powerful behavioral effects? Here, we use dual dendritic and somatic recordings in acute hippocampal slices of male mice to reveal that dendritic spike propagation, but not spike initiation, is strongly enhanced when the somatic resting potential is depolarized, likely as a result of increased inactivation of A-type $K^+$ channels. Somatic depolarization also facilitates the induction of a form of dendritic spike driven heterosynaptic plasticity that enhances memory specificity. Thus, the effect of somatic membrane depolarization to enhance dendritic spike propagation and long-term synaptic plasticity is likely to play an important role in hippocampal-dependent spatial representations as well as learning and memory.**

*Key words:* **calcium spike; dendrite; hippocampus; plasticity; pyramidal neuron; synaptic integration**

**Significance Statement**

**Neurons receive synaptic input along their dendrites but produce action potential (AP) output at their soma. Signals arriving at the distal dendrites of pyramidal neurons (PNs) have little impact on the soma unless they combine to initiate a dendritic spike, which needs to propagate to the soma to trigger an AP. This study shows that small subthreshold depolarization of the soma powerfully enhances the propagation of dendritic spikes, through inactivation of dendritic A-type potassium channels. Enhanced dendritic spike propagation also markedly facilitates the induction of a form of plasticity driven by the distal synaptic inputs. Thus, small changes in somatic membrane potential, similar to those observed *in vivo*, act as a powerful gate of neuronal information transfer.**

## Introduction

Pyramidal neurons (PNs) are the principal excitatory cells within the brain and process information from thousands of inputs from different brain regions to generate an action potential (AP) output. One common motif of synaptic organization is that long-range inputs from distant brain regions often target the most distal regions of a PN's apical dendrites, whereas local excitatory inputs target regions closer to the soma (Larkum, 2013). As a result of this dendritic organization, local and long-range inputs differentially trigger AP output. Whereas the local inputs produce large suprathreshold somatic EPSPs, long-range inputs generate very small subthreshold EPSPs at the soma because of attenuation by the dendritic cable. Nonetheless distal inputs are thought to play important roles in regulating neural activity, in part, because the active properties of dendrites enable the distal inputs to trigger the firing of distal dendritic spikes (Stuart and Spruston, 2015). Such distally-generated dendritic spikes have been implicated in hippocampal-dependent learning (Golding et al., 2002; Mehta, 2004; Kaifosh and Losonczy, 2016), place field generation (Bittner et al., 2015), and neocortical-mediated sensory perception (Takahashi et al., 2016; Manita et al., 2017).

In the hippocampus, CA1 PNs receive both direct long-range connections from the entorhinal cortex that target CA1 distal dendrites and local connections from the hippocampal CA3

Received Apr. 9, 2021; revised Feb. 2, 2022; accepted Mar. 1, 2022.

Author contributions: T.B. and S.A.S. designed research; T.B. and A.N. performed research; T.B. and A.N. analyzed data; T.B. wrote the first draft of the paper; T.B., A.N., and S.A.S. edited the paper; T.B. and S.A.S. wrote the paper.

This work was supported by the National Institutes of Health. We thank the members of the Siegelbaum lab for helpful discussions and Prof. Attila Losonczy for his input and helpful comments.

The authors declare no competing financial interests.

Correspondence should be addressed to Tobias Bock at htb2110@columbia.edu.

https://doi.org/10.1523/JNEUROSCI.0780-21.2022

Schaffer collaterals (SCs) that target CA1 proximal dendrites (Kajiwara et al., 2008). Genetic and chemical lesion studies suggest that the distal inputs are important for temporal (Suh et al., 2011) and contextual memory (Basu et al., 2016) and play a role in fine-tuning CA1 place field firing (Brun et al., 2008). Although dendritic spikes help boost the influence of these distal inputs at the CA1 soma, recordings from both acute hippocampal slices and computational modeling indicate that CA1 dendrites powerfully attenuate these spikes, limiting their influence to only a small subthreshold depolarization (Jarsky et al., 2005; Sun et al., 2014).

How can we reconcile the behavioral importance of the distal inputs with their weak somatic excitation? Although dendritic spikes on their own produce only a small subthreshold somatic depolarization, they can interact with more proximal excitatory inputs to trigger the firing of bursts of somatic APs termed complex spikes (Jarsky et al., 2005; Takahashi and Magee, 2009). Active dendritic spikes also provide an important source of $Ca^{2+}$ entry for generating long-term synaptic plasticity at distal synapses (Golding et al., 2002; Takahashi and Magee, 2009). Finally, dendritic spikes have been proposed to serve as instructive signals by mediating a heterosynaptic form of plasticity termed input-timing-dependent plasticity (ITDP), in which dendritic spikes triggered by distal inputs produce a long-term enhancement of CA1 excitation by the SC inputs (Dudman et al., 2007; Basu et al., 2013), thereby enhancing the specificity of contextual memory (Basu et al., 2016).

In addition to being regulated by coincident proximal synaptic stimulation, several lines of evidence suggest that distal synaptic inputs may exert a surprisingly large influence on somatic output under *in vivo* conditions. Thus, CA1 neurons show relatively normal rates of place cell firing when proximal SC inputs are lesioned (Brun et al., 2002) or genetically silenced (Nakashiba et al., 2008), which has been attributed to a high efficacy of the remaining influence of the distal inputs. What might be responsible for the apparent greater efficacy of distal synaptic inputs in triggering somatic output under *in vivo* conditions compared with *ex vivo* slices?

Here, we examine the potential influence of somatic resting potential on the generation and propagation of distal dendritic spikes since the soma often experiences significant subthreshold depolarizations *in vivo* as a result of excitatory input. Subthreshold fluctuations in somatic membrane potential have been shown to exhibit modulatory effects on actively propagating signals, such as backpropagating APs (bAPs) and axonic APs in dentate gyrus granule cells (Alle and Geiger, 2006; Brunner and Szabadics, 2016). The importance of somatic voltage for *in vivo* neural activity has been previously established by the finding that small depolarizations from the resting potential promote the firing of complex spikes (Grienberger et al., 2014) and lead to the *de novo* appearance of CA1 place field firing in formerly silent neurons (Lee et al., 2012). Larger depolarizations promote the firing of long-lasting dendritic plateau potentials that generate *de novo* place fields (Bittner et al., 2015), presumably by triggering synaptic plasticity.

However, the mechanism by which somatic depolarization may amplify distal synaptic inputs remains incompletely understood. A recent study found that in rat hippocampal slices somatic depolarization can amplify the response at the CA1 neuron soma to a subthreshold burst of distal EPSPs as a result of the activation of a perisomatic persistent voltage-dependent $Na^+$ conductance (Hsu et al., 2018). A previous study reported that somatic depolarization also enhances the propagation of suprathreshold dendritic spikes in CA1 PNs in isolated rat hippocampal slices (Gasparini et al., 2004). However, the mechanism by which weak somatic depolarization alters dendritic spike propagation and dendritic-spike-dependent forms of plasticity is not fully understood. Here, we report that somatic depolarization in mouse CA1 PNs powerfully enhances the propagation of distal dendritic spikes, but not subthreshold EPSPs, by enhancing the resting inactivation of dendritic A-type voltage-gated potassium ($K^+$) channels. Furthermore, somatic depolarization dramatically enhances the efficacy of induction of ITDP, an effect that is due, at least in part, to the enhancement of dendritic spike propagation, providing a potential mechanism for regulating the specificity and strength of hippocampal-dependent declarative memory.

## Materials and Methods

*Slice preparation*

Male C57Bl/6J mice (7–12 weeks old) were anesthetized by inhalation of isoflurane (5%) for 7 min, subjected to cardiac perfusion of cold artificial CSF (ACSF) for 30 s before decapitation according to the procedures approved by the IACUC of Columbia University and the New York State Psychiatric Institute. The skull was opened and the brain removed and immediately transferred into ice-cold carbogenated ACSF (in mM; 22.5 glucose, 125 NaCl, 1 $MgCl_2$, 2 $CaCl_2$, 25 $NaHCO_3$, 3 KCl, and 1.25 $NaH_2PO_4$, pH 7.2). During the slicing procedure, the $MgCl_2$ concentration was increased to 4 mM to reduce cell excitability. The hippocampus was dissected in both hemispheres; 400-μm-thick horizontal hippocampal slices were cut using a vibrating tissue slicer (VTS 1200, Leica) and transferred to a chamber containing ACSF at 35°C, where they were incubated for 40 min. Thereafter, slices were held at room temperature (21°C) until transfer into the recording chamber.

*Electrophysiology*

Slices were transferred from the incubation chamber into the recording chamber of an Olympus BX51WI microscope (Olympus), where they were either held in place by a 1 mm grid of nylon strings on a platinum frame or, in the case of experiments that required dual extracellular stimulation, by pinning the slice to the bottom of the chamber with the two stimulation electrodes. Slices were continually perfused with ACSF at a temperature of 34 ± 1°C, maintained by a thermostat-controlled flow-through heater (Warner Instruments)

In the case of single somatic recordings, healthy somas of CA1 PNs were identified visually under 80× (40 × 2) magnification and patched under visual guidance using borosilicate glass pipettes [inner diameter (i.d.) 0.75 mm, outer diameter (o.d.) 1.5 mm, Sutter Instruments] with a tip resistance of 4–5.5 MΩ, connected to a Multiclamp 700B amplifier (Molecular Devices) and filled with intracellular solution, containing (in mM): 135 K-gluconate, 5 KCl, 0.2 EGTA, 10 HEPES, 2 NaCl, 5 MgATP, 0.4 $Na_2GTP$, and 10 $Na_2$-Phosphocreatin, adjusted to a pH of 7.2 with KOH. Recordings were only accepted if the series resistance after establishing a whole-cell configuration did not exceed 22 MΩ and did not change by >20% of the initial value during the course of the experiment.

In the case of single dendritic patches, a thick-walled borosilicate glass pipette (i.d. 0.75 mm, o.d. 1.6 mm) with a tip resistance of 9–13 MΩ was lowered slowly (<2 μm/s) into the distal stratum radiatum (SR) of CA1. Dendrites were patched blindly by tracking changes in the tip resistance. Recordings were included into the analysis if the series resistance after establishing whole-cell configuration did not exceed 45 MΩ and if it did not change by >20% of the initial value during the course of the experiment.

In the case of dual dendritic and somatic patch clamp recording, both methods described above were combined, starting with the dendritic blind patch. In this case, 5 μM Alexa Fluor 594 fluorescent dye (ThermoFisher Scientific) was added to the intracellular solution of the dendritic patch pipette to visualize the soma of the same cell and target it for the somatic patch clamp.

In the case of localized extracellular synaptic stimulation, stimulator pipettes were pulled from borosilicate glass capillaries (i.d. 0.75 mm, o.d. 1.5 mm, Sutter Instruments) with a tip resistance of 5–7 MΩ. These pipettes were filled with 1 M NaCl solution, attached to electrode holders, connected to a separate grounding electrode in the bath and inserted into the slice in SR (for SC stimulation) or stratum lacunosum moleculare (SLM; for PP stimulation) at a distance of at least 180 µm from the patched cell and/or dendrite to avoid direct electrical stimulation of the patched cell. Stimulations were administered through battery powered stimulator boxes, connected to the stimulation and ground electrodes and triggered via TTL signals.

*Pharmacology*

Drugs were prepared as stock solutions and stored until needed. They were then diluted to final concentration in ACSF and added to the bath. Tetrodotoxin (TTX; Sigma-Aldrich) was stored as a stock solution of 1 mM in ACSF at −20°C and applied at 500 nM to the bath. $Cd^{2+}$ (Sigma-Aldrich) was stored as a stock solution of 100 mM $CdCl_2$ in ACSF at 4°C and applied to the bath at 200 µM. 4-aminopyridine (4-AP; Tocris) was stored as a stock solution of 100 mM in ACSF at −20°C and applied to the bath at 5 mM. Phrixotoxin-2 (Alomone Labs) was stored at a stock concentration of 5 µM and bath applied at a concentration of 500 nM. SR95531 (Tocris) was stored as a stock solution of 20 mM in ACSF at −20°C and applied to the bath at a concentration of 2 µM. CGP55845 (Tocris) was stored as a stock solution of 10 mM at −20°C and applied to the bath at 1 µM. AM251 (Tocris) was stored in a stock solution of 20 mM in DSMO and added to the bath at a concentration of 2 µM.

*Data acquisition and analysis*

Electrophysiological recordings were digitized, using a Digidata 1322A A/D interface (Molecular Devices), at a sampling rate of 20 kHz (low pass filtered at 10 kHz) and recorded using pClamp 10 software (Molecular Devices). The amplifier settings of the Multiclamp 700B were controlled through Multiclamp Commander (Molecular Devices). In one experiment a custom designed script, built on the basis of Ephus software (Suter et al., 2010) was used to perform online analysis and insert a negative current into the cell, based on the membrane voltage (Fig. 9*I*).

Data were analyzed using Axograph X software (Axograph Scientific), MATLAB (MathWorks) as well as Microsoft Excel (Microsoft Corp.). Prism 4/5 (GraphPad) was used for statistics and preparation of graphs. For paired data Wilcoxon's nonparametric matched pairs test or a paired *t* test (if a Gaussian distribution could be assumed) was used to test statistical significance unless otherwise noted. For multiple datasets Dunn's multiple comparison test was performed to determine statistical significance unless otherwise noted. Results are presented as average values ± SE. Data were presented in Acrobat Illustrator (Adobe). Example traces represent raw data recordings with electrical artifacts of extracellular stimulation downscaled to 3–15%.

Baseline and steady state membrane potentials were calculated as averages over the baseline period before the first current injection (minimum of 50 ms) or steady state period (minimum 25 ms). Amplitudes were measured by averaging the membrane potential over a 1-ms window around the peak (to reduce the impact of noise), relative to the corresponding steady state (either baseline or the steady state of the underlying current step). Active signals (both dendritic spikes and somatic APs) were detected when the derivative of the membrane potential exceeded 50 mV/ms, excluding extracellular stimulus artifacts. Additionally, all somatic and dendritic spikes were verified manually during the analysis.

*Computational modeling*

To generate a computational model of the effects observed in the electrophysiological experiments, a simplified representation of a CA1 pyramidal cell was created, using the NEURON environment (Hines and Carnevale, 1997) and a custom generated Python based overlay script. The PN representation consists of a spherical soma with a diameter of 20 µm, an apical dendritic trunk with a length of 400 µm and a diameter of 2 µm and another 20-µm spherical compartment, representing the accumulated apical tuft dendrites. Passive properties of these three compartments were adjusted individually to best represent the observed electrophysiological data of CA1 PNs in acute brain slices (Figs. 1, 2; Tables 1, 2). The following channels were added to the three compartments: R-type and T-type calcium channels were added to the tuft and trunk compartments with a conductance gradually decreasing toward the soma (Magee and Carruth, 1999; Iftinca et al., 2006; Neumaier et al., 2020). A-type $K^+$ channels were added into the soma at low conductance but with an increasing gradient along the apical trunk, peaking at 280-µm distance from the soma (Hoffman and Johnston, 1999; Migliore et al., 1999; Kerti et al., 2012). HCN channels were added in all compartments with a conductance gradient increasing toward the dendritic tuft (Santoro et al., 1997; Magee, 1998). Delayed rectifier $K^+$ channels were added to the somatic compartment (Migliore et al., 1999). Internal calcium dynamics and pump were modeled as an exponential decay formula (Destexhe et al., 1993). Based on this calculation of the internal calcium concentration, a calcium sensitive K channel was implemented in the dendritic compartments to help repolarize the dendritic plateau potential (Moczydlowski and Latorre, 1983; Cai et al., 2004). No voltage gated sodium channels were added to the model, as we modeled the propagation mechanism in the presence of TTX (Figs. 1, 2).

Conductances were initially set to reflect previous modeling and empirical data on these channels in mouse models where available or in rat models if not (Magee and Carruth, 1999; Migliore et al., 1999; Poirazi et al., 2003; Golding et al., 2005; Neumaier et al., 2020) and were then adjusted to best reproduce the observed data (see Table 3).

**Data availability**

The datasets generated and analyzed during the current study are available at https://drive.google.com/drive/folders/1ANHQhYiUdb6jvS-NzBVnqwINx5ry5YfA?usp=sharing.

**Code availability**

The computational model code is available at ModelDB (https://senselab.med.yale.edu/ModelDB/). Model number: 267311.

## Results

### Dendritic spike propagation efficacy is modulated by the somatic membrane potential

To explore the regulation of dendritic spike propagation in hippocampal CA1 PNs, we obtained dual whole-cell current clamp recordings from the soma and distal apical dendrite of these cells, ~250–300 µm from the soma (at the border of SR and SLM), in acute hippocampal slices from adult mice (Fig. 1*A*). We triggered a distal dendritic spike by injecting a 350-pA, 100-ms depolarizing current step through the dendritic patch pipette and recorded the resultant voltage change at the soma (Fig. 1*B*). In the dendrite, the resultant spike had a fast rising component, typically associated with voltage-gated $Na^+$ channels (Kim and Connors, 1993; Golding and Spruston, 1998), followed by a slower plateau potential, typically generated by voltage-gated $Ca^{2+}$ channels (Amitai et al., 1993; Kim and Connors, 1993; Schiller et al., 1997; Golding et al., 1999). When the somatic membrane potential was held initially at −70 mV, near the typical CA1 resting potential, the dendritic spike (32.4 ± 5.3 mV in amplitude) produced only a very small somatic depolarization (0.65 ± 0.08 mV, $n = 5$; Fig. 1*B–D*), for a dendritic attenuation factor (the amplitude of the peak somatic depolarization during the dendritic current step, divided by the peak amplitude of the dendritic spike) of 49.8 ± 5.7, consistent with previous findings (Jarsky et al., 2005; Sun et al., 2014) .

However, depolarization of the somatic resting potential by constant current injection dramatically enhanced the efficacy of dendritic spike propagation by nearly an order of magnitude. Thus, with the soma held initially at −55 mV, a distal dendritic spike

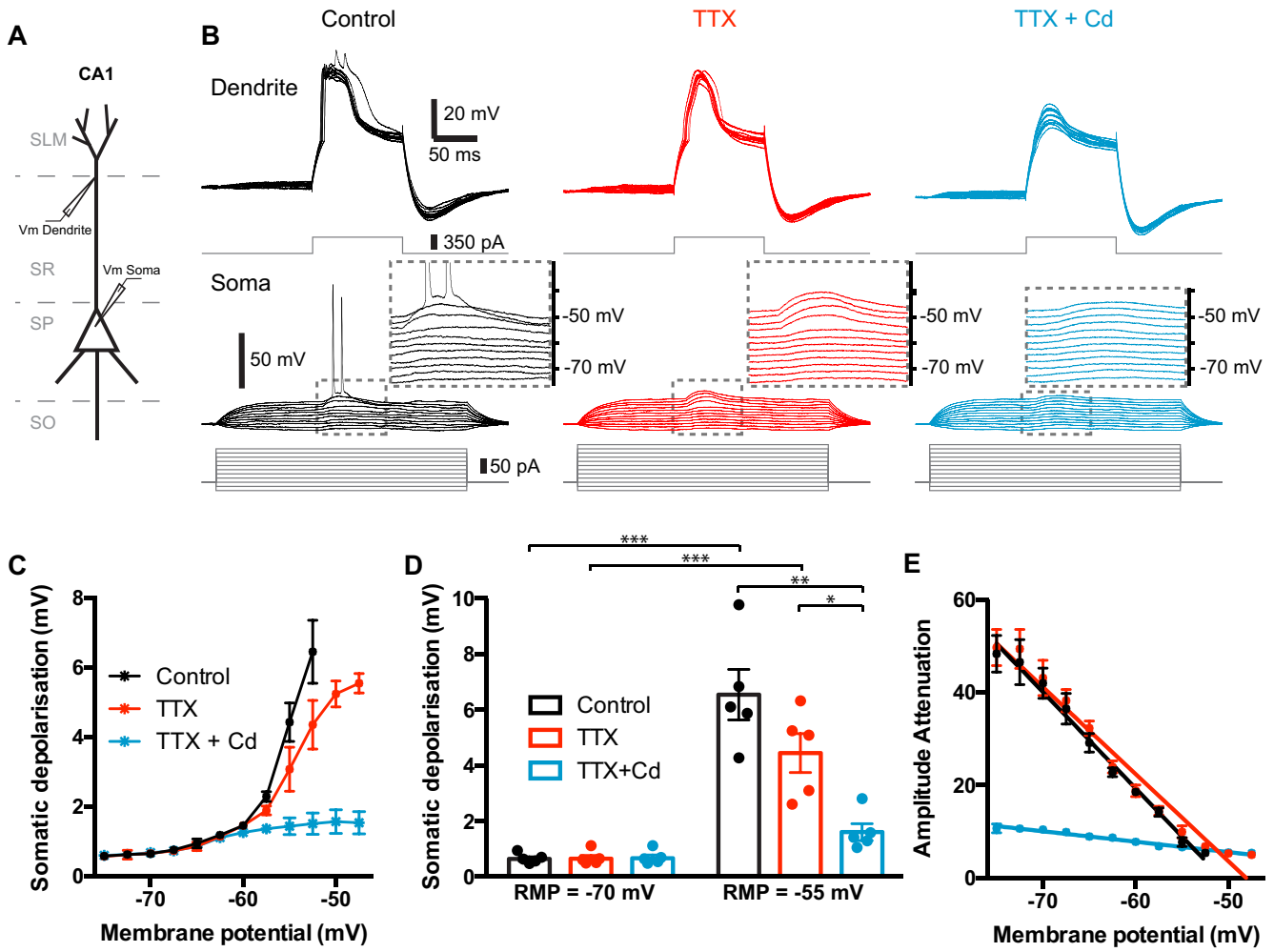


**Figure 1.** Somatic resting membrane potential determines the efficacy of dendritic spike propagation to the soma. ***A***, Schematic of the experimental setup. ***B***, Dendritic (top) and somatic (bottom) recording of a dendritic spike, elicited by current injection into the dendrite at varying somatic membrane potentials before (black) and after adding 500 nM TTX (red) followed by 200 $\mu$M Cd (blue) to the bath solution; insets show an expanded view of the traces within the dashed box. ***C***, Peak depolarization of the somatic membrane potential in response to a dendritic spike at varying somatic baseline potentials before (black) and after adding TTX (red) and Cd (blue) to the bath. ***D***, Comparison of peak somatic membrane depolarization at −70- and −55-mV baseline somatic membrane potential before (black) and after adding TTX (red) and Cd (blue) to the bath, all data are paired as all conditions were recorded consecutively in each of the patch-clamped cells. ***E***, Attenuation factor of the dendritic calcium spike, as it propagates to the soma, plotted against the somatic baseline potential before (black) and after adding TTX (red) and cadmium (blue) to the bath. *$p < 0.05$, **$p < 0.01$, ***$p < 0.001$; multiple t-test after 2way ANOVA.

produced a 6.46 ± 0.90 mV somatic depolarization, decreasing the attenuation factor to 7.79 ± 1.19 ($p < 0.005$, $n = 5$; Fig. 1*B–D*). Upon further depolarization of the soma, a dendritic spike typically elicited a burst of somatic APs (Fig. 1*B*). Changes in somatic membrane potential had no impact on dendritic spike threshold, amplitude or duration at the distal dendritic recording site (Table 1). Somatic depolarization also caused no significant change in the passive properties of the cell in either compartment (Table 1). The signal attenuation factor between the distal dendritic recording site and the soma showed an S-shaped dependence on membrane potential, decreasing continuously to an asymptotic value as the somatic membrane potential was depolarized ($p < 0.0001$ with Friedman test, $n = 5$; Fig. 1*E*). We term this phenomenon depolarization enhancement of dendritic spike propagation (DEDSP).

To determine the ionic nature of the dendritic spikes and the mechanism by which somatic depolarization enhanced their propagation, we examined the effects of antagonists of voltage-gated $Na^+$ and $Ca^{2+}$ channels. Inhibition of voltage-gated $Na^+$ channels with TTX (500 nM) blocked the fast phase of the dendritic spike but left the slower plateau potential unchanged (indicative of $Ca^{2+}$ spikes; Amitai et al., 1993; Kim and Connors, 1993; Schiller et al., 1997; Golding and Spruston, 1998; Golding et al., 1999). Somatic depolarization enhanced the propagation to the soma of these $Ca^{2+}$ spikes in a manner similar to that seen under control conditions. In TTX, the somatic amplitude of the dendritic spike was 0.66 ± 0.13 mV at a somatic resting potential of −70 mV compared with 4.36 ± 0.69 mV at a resting potential of −55 mV ($p < 0.05$, $n = 5$; Fig. 1*B–D*), indicating that DEDSP does not require voltage-gated $Na^+$ channels. Combined application of the voltage-gated $Ca^{2+}$ channel blocker $Cd^{2+}$ (200 $\mu$M) and TTX fully eliminated the dendritic spike, even in the distal dendrite (0.69 ± 0.11 mV at −70 mV vs 1.51 ± 0.31 mV at −55 mV, $p = 0.07$; Fig. 1*B–D*), confirming that the plateau potentials were $Ca^{2+}$ spikes. Importantly, with dendritic spikes blocked, somatic depolarization had only a minimal effect on propagation of the passive dendritic depolarization.

### Modulation of dendritic spike propagation efficacy during somatic membrane depolarization is dependent on A-type $K^+$ channels

Previous studies have implicated voltage-gated A-type Kv4.2/4.3 $K^+$ channels in regulating dendritic excitability. These channels

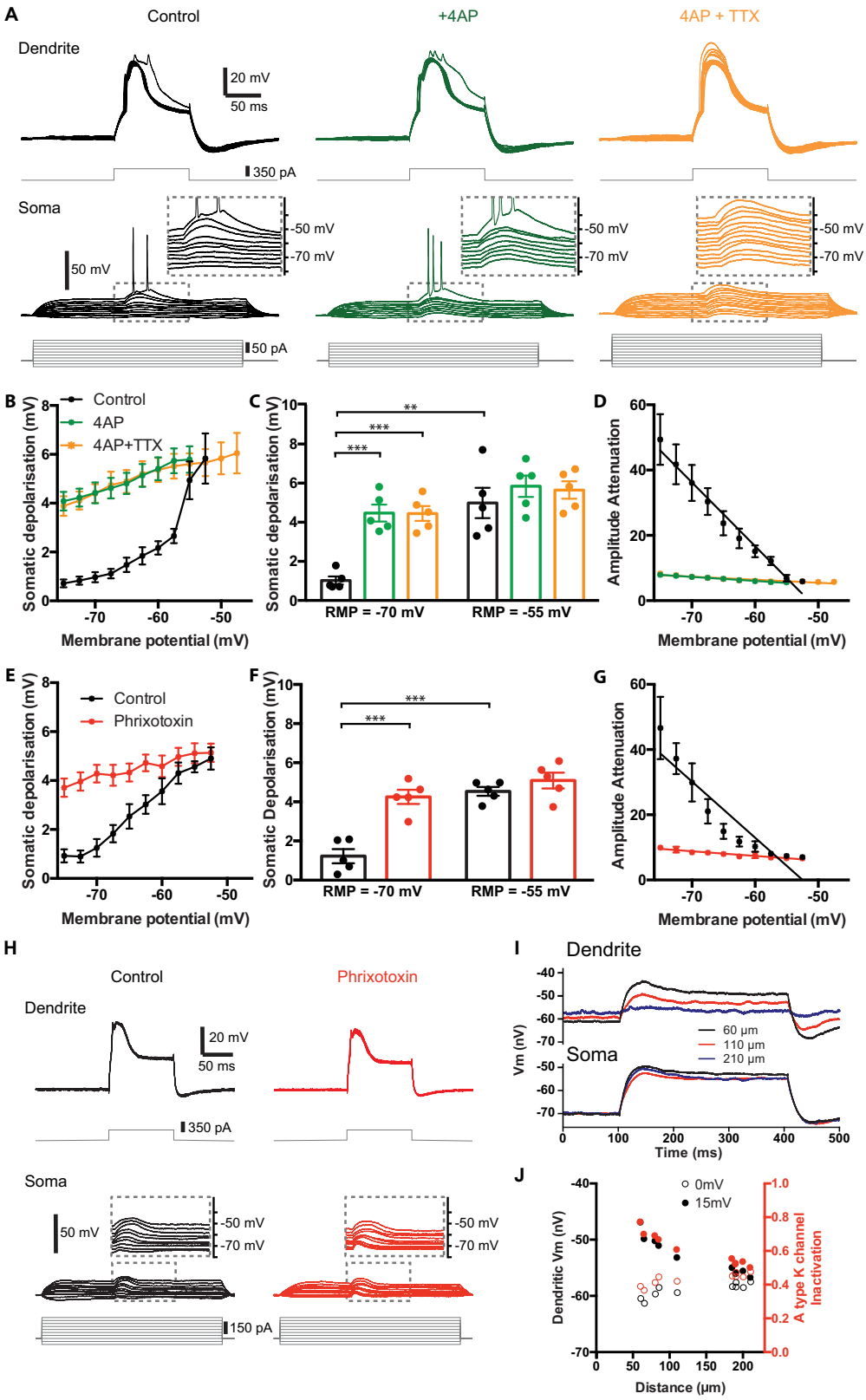


**Figure 2.** The voltage dependence of the propagation efficacy of dendritic spikes is mediated by 4-AP-sensitive and phrixotoxin-2-sensitive $K^+$ channels. ***A***, Dendritic (top) and somatic (bottom) recording of a dendritic spike, elicited by current injection into the dendrite at varying somatic membrane potentials before (black) and after adding 5 mM 4-AP (green) and 500 nM TTX (orange) to the bath solution, insets show a zoom of the traces of somatic membrane potential within the squares. ***B***, Peak depolarization of the somatic membrane potential during the dendritic spike at varying somatic baseline potentials before (black) and after adding 4-AP (green) and TTX (orange) to the bath. ***C***, Comparison of peak somatic membrane depolarization at −70- and −55-mV baseline somatic membrane potential before (black) and after adding 4-AP (green) and TTX (orange) to the bath; all data are paired as all conditions were recorded consecutively in each of the patch-clamped cells. ***D***, Attenuation factor of the dendritic calcium spike, as it propagates to the soma, plotted against the somatic baseline potential before (black) and after adding 4-AP (green) and TTX (orange) to the bath. ***E–G***, Same as ***B–D*** but comparing data before (black) and after (red) application of 500 nM phrixotoxin-2. ***H***, Dendritic (top) and somatic (bottom) recording of a dendritic spike, elicited by current injection into the dendrite at varying somatic membrane potentials before (black) and after adding 500 nM phrixotoxin-2 (red).

**Table 1. Membrane and spike properties of CA1 PNs, analyzed in Figure 1 ($n = 6$)**

| Property | Location | No drugs | +TTX | +TTX and Cd | Vm at −55 mV |
|---|---|---|---|---|---|
| Resting membrane potential (mV) | Soma | −67.6 ± 1.2 | −67.3 ± 1.0 | −66.0 ± 1.4 | — |
| | Dendrite | −59.5 ± 1.9 | −58.7 ± 1.4 | −58.4 ± 1.3 | — |
| Input resistance (MΩ) | Soma | 102.8 ± 6.0 | 103.7 ± 7.0 | 108.1 ± 6.2 | 101.2 ± 7.5 |
| | Dendrite | 76.6 ± 2.5 | 77.6 ± 2.0 | 86.2 ± 1.8 | 69.4 ± 4.1 |
| Dendritic spike amplitude (mV) | Dendrite | 58.6 ± 5.1 | 48.6 ± 4.3 | 20.5 ± 1.5 | 53.5 ± 4.7 |
| Dendritic spike half width (ms) | Dendrite | 30.3 ± 2.1 | 28.6 ± 1.7 | 12.9 ± 1.2 | 32.7 ± 3.0 |
| AP threshold (mV) | Soma | −45.4 ± 0.7 | — | — | −45.5 ± 0.6 |
| Dendritic spike threshold (mV) | Dendrite | −33.5 ± 1.5 | −31.7 ± 1.8 | — | −33.2 ± 1.5 |

**Table 2. Membrane and spike properties of CA1 PNs, analyzed in Figure 2*A–D* ($n = 6$)**

| Property | Location | No drugs | +4-AP | +4-AP and TTX |
|---|---|---|---|---|
| Resting membrane potential (mV) | Soma | −65.1 ± 0.8 | −63.2 ± 1.3 | −62.9 ± 1.3 |
| | Dendrite | −53.9 ± 1.9 | −51.9 ± 2.9 | −51.3 ± 1.7 |
| Input resistance (MΩ) | Soma | 106.5 ± 9.5 | 111.7 ± 8.1 | 116.3 ± 8.3 |
| | Dendrite | 74.2 ± 3.0 | 78.0 ± 3.9 | 79.8 ± 4.7 |
| Dendritic spike amplitude (mV) | Dendrite | 62.7 ± 6.8 | 67.6 ± 7.3 | 59.8 ± 8.0 |
| Dendritic spike half width (ms) | Dendrite | 37.8 ± 4.8 | 42.9 ± 3.7 | 45.3 ± 4.3 |
| AP threshold (mV) | Soma | −40.4 ± 0.7 | −40.3 ± 0.6 | — |
| Dendritic spike threshold (mV) | Dendrite | −36.0 ± 1.3 | −38.6 ± 0.8 | −37.0 ± 1.7 |

**Table 3. Ion channel conductances in the three compartments of the NEURON model of a simplified CA1 PN**

| Conductance (S/cm$^2$) | Tuft | Trunk | Soma |
|---|---|---|---|
| Passive leak | 1e-3 | 7e-4 to 1e-3 | 6e-4 |
| Delayed rectifier (KDR) | 5e-4 | 2e-3 to 5e-4 | 2e-3 |
| A-type $K^+$ channel | 1e-3 | 3e-2 to 5e-4 at trunk(0.7) | 1e-4 |
| R-type $Ca^{2+}$ (density in channels/cm$^2$) | 3.1e10 | 1e7 to 2.4e10 | 0 |
| T-type $Ca^{2+}$ | 2e-6 | 1e-7 to 2e-5 | 0 |
| K(Ca) channel (mAHP) | 3.5e-4 | 1e-5 | 1e-6 |
| HCN | 6e-3 | 8e-4 to 6e-3 | 8e-4 |

are present in the apical dendrites of CA1 PNs where they regulate the back-propagation of somatic APs (Hoffman et al., 1997; Gasparini et al., 2007), curtail the duration of dendritic plateau potentials, and confine their spread throughout different dendritic branches (Cai et al., 2004). Moreover, these channels rapidly inactivate over a voltage range that matches the effect of somatic depolarization we observed (Hoffman et al., 1997; Ramakers and Storm, 2002; Kim et al., 2007), providing a potential mechanism for how depolarization may enhance dendritic spike propagation.

To examine directly the role of A-type $K^+$ channels in DEDSP, we compared the effects of membrane depolarization on dendritic spike propagation before and after bath application of the A-type $K^+$ channel blocker, 4-AP (5 mM). Application of 4-AP greatly enhanced spike propagation at a somatic holding potential of −70 mV and largely occluded the enhancement in spike propagation with membrane depolarization (Fig. 2*A–D*). Although some residual effect of depolarization on propagation efficacy remained in the presence of 4-AP ($p < 0.005$ with Friedman test; Fig. 2*B*,*D*), nonlinear fits to the data showed that 4-AP significantly diminished the effect of voltage ($p < 0.01$ with extra-sum-of-squares $F$ test; Fig. 2*B*,*D*). In the presence of 4-AP, the slope of a linear regression of the dendritic attenuation curve (Fig. 2*D*) was reduced by 93.8%, from −1.94 to −0.12 ($p < 0.0001$). Furthermore, while somatic depolarization from −70 to −55 mV caused a large and highly significant increase in the amplitude of the dendritic spike at the soma (0.97 ± 0.2 mV compared with 4.94 ± 0.78 mV; $p < 0.005$, $n = 5$; Fig. 2*C*), depolarization caused only small, nonsignificant increase in the somatic response in the presence of 4-AP (4.42 ± 0.43 vs 5.79 ± 0.55 mV; $p = 0.063$, $n = 5$; Fig. 2*C*). Finally, 4-AP produced a similar enhancement of dendritic $Ca^{2+}$ spike propagation in the presence of TTX, confirming that voltage-gated $Na^+$ channels are not required (Fig. 2*B–D*).

As 4-AP is also known to block Kv1 delayed-rectifier channels (Castle et al., 1994), we examined the effect of the specific Kv4.2/3 blocker phrixotoxin-2 (Diochot et al., 1999; Chagot et al., 2004). Under control conditions, the somatic depolarization in response to a dendritic spike increased significantly from 1.26 ± 0.36 mV at a somatic membrane potential of −70 to 4.56 ± 0.26 mV when the somatic membrane was depolarized to −55 mV ($p < 0.005$, $n = 5$; Fig. 2*E–H*). Similar to the action of 4-AP, 500 nM phrixotoxin-2 caused a significant increase in the amplitude of the somatic response to a dendritic spike at a somatic resting potential of −70 mV (4.28 ± 0.37 mV; $p < 0.005$ vs control in absence of phrixotoxin-2, $n = 5$). Moreover, the enhancement in dendritic spike propagation normally seen on depolarization of the membrane to −55 mV was largely abolished by the toxin (5.12 ± 0.41 mV at – 55 mV, $p = 0.094$, $n = 5$; Fig. 2*F*), with the slope of the best linear fit to the somatic response–voltage relation reduced by 91.6%, from 1.67 to 0.14 ($p < 0.0001$ with linear regression test; Fig. 2*G*).

Since neither 4-AP nor phrixotoxin-2 altered dendritic passive membrane properties, dendritic spike threshold, amplitude or duration (Table 2), we surmised that somatic depolarization might enhance dendritic spike propagation by enhancing the resting inactivation of A-type $K^+$ channels. As a first test of this

←

***I***, Voltage traces in 3 example cells, patch-clamped at the soma and recorded from at different dendritic locations (black, 60-µm distance from soma; red, 110-µm distance; blue, 200-µm distance) in response to a 300-ms somatic current step (100–400 ms), adjusted in each cell to provide ~15-mV somatic depolarization. ***J***, Depolarization (black) with estimated A-type $K^+$ channel availability according to Hoffman et al. (1997); (steady-state inactivation shown in red) at various dendritic locations when the soma is depolarized by 15 mV (closed circles) or when the soma is not depolarized (open circles). $^{**}p < 0.01$, $^{***}p < 0.001$; multiple t-test after 2way ANOVA.

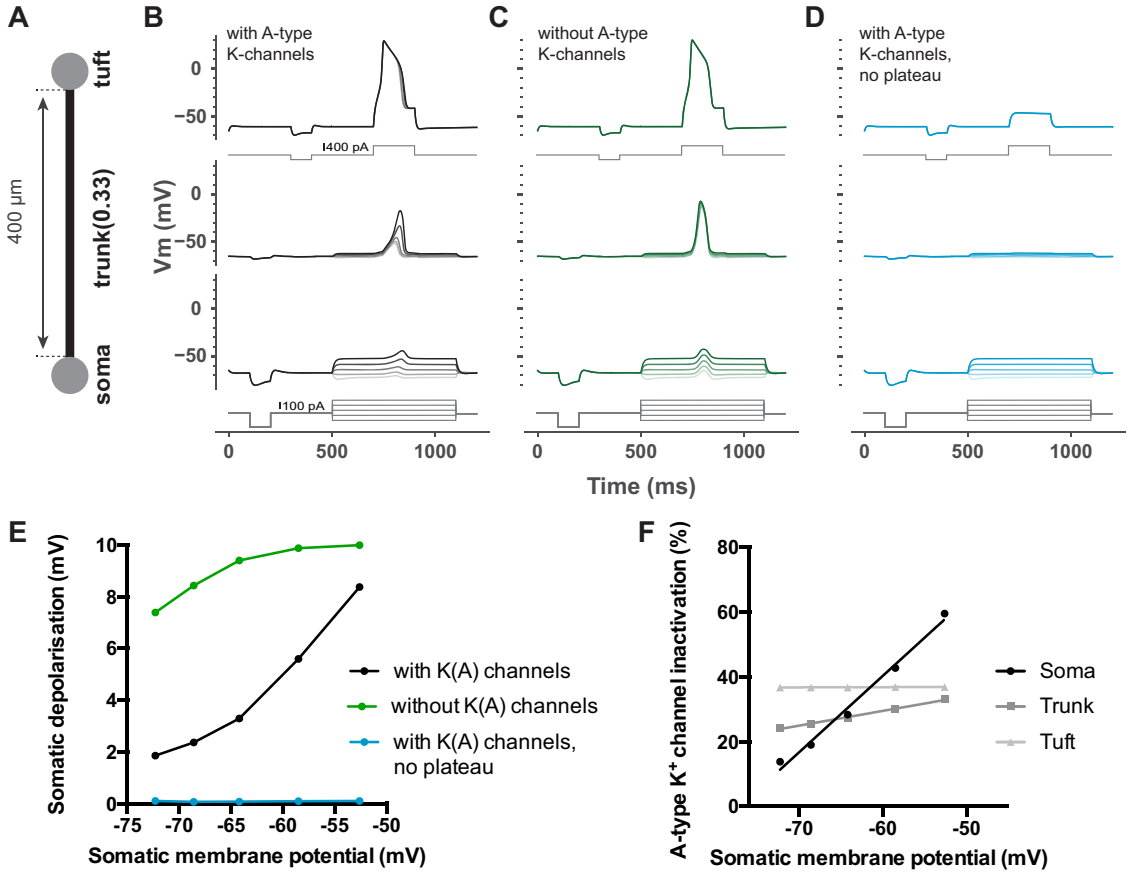


**Figure 3.** Computational model of a three compartment CA1 PN, reproducing key features of DEDSP. ***A***, Schematic of the three-compartment model. ***B***, Voltage traces recorded from the tuft (top), trunk (at position 0.33 where the soma is 0 and the tuft is 1, middle), and soma (bottom) in response to a 500-pA current step injected into the tuft compartment (top gray current traces) while the somatic membrane potential was modified by long-lasting current steps into the soma, ranging from −100 to +200 pA (bottom gray current traces). ***C***, Same as ***B*** except that the A-type $K^+$ conductance was set to 0 (simulating block of A-type $K^+$ channels). ***D***, Same as ***B***, except that the dendritic current injection was reduced to 250 pA to generate a subthreshold event in the tuft compartment. ***E***, Peak depolarization of the somatic membrane in response to the dendritic spike at varying somatic membrane potentials before the dendritic spike onset (measured at 700 ms during the simulations shown in ***B***, ***C***) with a realistic level of A-type $K^+$ channel conductance (black), with the A-type $K^+$ conductance set to 0 (green), and in response to a subthreshold dendritic current injection with A-type $K^+$ channels present (blue). ***F***, The percentage of inactivated A-type $K^+$ channels in the soma (black), trunk (at position 0.33, dark gray) and tuft (light gray) at varying somatic membrane potentials (measured at 700 ms during the simulations shown in ***B***, ***C***). Lines depict linear regression fits.

idea, we measured the effects of somatic depolarization on the proximal dendritic membrane voltage of CA1 PNs to determine whether the extent of depolarization was likely sufficient to alter channel inactivation. We performed multiple dual patch clamp recordings from the soma and from the apical dendrite at various distances from the soma. In each cell, we injected 300-ms current steps into the soma to depolarize the somatic membrane voltage by ~15 mV while recording from the apical dendrites. Consistent with previous observations on spatial attenuation of voltage changes (Bar-Yehuda and Korngreen, 2008), we saw a strong depolarizing effect of a 15-mV somatic depolarization on the proximal dendrites, but little effect in the distal dendrites (Fig. 2*I*, *J*). Using the inactivation vs voltage plot for A-type $K^+$ channels from Hoffman et al. (1997) and correcting for liquid junction potential (−6.2 mV), we found that the measured effect of somatic depolarization should markedly increase steady-state inactivation of the A-type $K^+$ channels in the proximal dendrites within 100–150 µm of the soma (Fig. 2*J*). Thus, in the proximal dendrite (60 µm from the soma), resting inactivation of A-type $K^+$ channels was predicted to increase from 38% when the soma was at −70 mV to 78% when the soma was depolarized to −55 mV. In contrast, in the distal dendrite (>200 µm from the soma), we expect only a small increase in resting inactivation, from 45% to 50% (Fig. 2*J*). From these data, we conclude that somatic depolarization should result in a marked increase in resting inactivation of A-type $K^+$ channels in the proximal apical dendrite that allows for more efficient propagation of dendritic spikes during somatic depolarization, while distal dendritic locations (the site of dendritic spike initiation) should be little affected by alterations in somatic voltage.

### A computational model shows the impact of A-type $K^+$ channels on propagating dendritic spikes in the apical trunk

To further explore the dynamics of the interaction between A-type $K^+$ channels and the propagation of the dendritic calcium spike, we created a three compartment NEURON model of a simplified pyramidal cell, including a soma, apical dendritic trunk, and apical dendritic tuft compartments (Fig. 3*A*; see Materials and Methods). Passive parameters were adjusted to reflect our experimental data on input resistance and time constant in all three compartments. Active conductances were distributed according to previous physiological and histochemical observations (see Materials and Methods) and consisted of R-type and T-type voltage-gated $Ca^{2+}$ channels, A-type $K^+$ channels, HCN channels, delayed rectifier $K^+$ channels, medium afterhyperpolarization Ca-dependent $K^+$ channels, and an exponentially decaying $Ca^{2+}$ extrusion mechanism. Voltage gated $Na^{2+}$ channels were not introduced into the model to minimize

the number of independently adjustable parameters as DEDSP was observed in the presence of TTX (Figs. 1, 2). This reduced model was able to reproduce the DEDSP phenomenon. Depolarization of the somatic resting membrane enhanced the amplitude of the dendritic spike at the soma, from 1.9 mV when the soma was held at −72.3 to 8.4 mV when the soma was depolarized to −52.5 mV, a 4.5-fold increase (Fig. 3*B*,*E*). Consistent with the experimental data, this change in the somatic depolarization was dependent on A-type $K^+$ channels. Reducing the A-type $K^+$ channel conductance to 0 greatly enhanced the somatic amplitude of the dendritic spike at the negative resting potential (7.4 mV when the soma was held at −72.3 mV) and markedly reduced the effect of somatic depolarization to enhance spike amplitude to a 1.3-fold increase (Fig. 3*C*,*E*). The model also reproduced our finding that DEDSP is dependent on actively propagating signals as a subthreshold dendritic depolarization is only minimally responsive to prior manipulation of the somatic membrane potential (Fig. 3*D*,*E*).

The modeling results also support the view that somatic depolarization enhanced dendritic spike propagation by increasing A-type $K^+$ channel inactivation. Increasing amounts of somatic depolarization that simulate our experimental values produced a progressive increase in channel inactivation that was much more pronounced in the soma and proximal dendrites than in the distal dendrites (Fig. 3*F*). In the soma, the fraction of A-type $K^+$ channels that were inactivated at a resting potential of −72 mV increased markedly when the soma was depolarized to −53 mV, from 0.14 to 0.60. The effect of somatic depolarization also enhanced A-type channel inactivation in the proximal portion of the apical dendrite (1/3 of the distance from the soma to tuft), from 0.24 to 0.33. These changes in inactivation in the soma and proximal dendrite were sufficient to have a large impact on spike regeneration along the trunk and thus the resulting depolarization seen in the soma.

The importance of A-type $K^+$ channel inactivation in enabling dendritic spike propagation was further supported by examining the effect of reducing inactivation by shifting the mid-point voltage of channel inactivation by 10 mV, from its normal value of −56 to −46 mV. This resulted in a nearly complete blockade of dendritic spike propagation, with little effect on spike generation at its point of origin in the tuft. Thus, the voltage shift in inactivation reduced the peak amplitude of the dendritic spike in the proximal apical dendrite from 14.5 to 5.0 mV with the soma held at −72.3 mV, and from 44.9 to 5.9 mV with the soma held at −52.5 mV. In contrast, the shift in inactivation only reduced spike amplitude in the tuft by 1.1 mV, from 89.9 to 88.8 mV (while changes of the somatic holding potential had a negligible effect of <0.05 mV in either case). It should be noted, that this model is meant to provide a proof-of-principle and to determine the likelihood that A-type $K^+$ channel inactivation contributes to the DEDSP mechanism. It is likely that other ion channels that were not included in the model may also contribute to this phenomenon.

### Somatic depolarization enhances propagation of synaptically evoked dendritic spikes but not subthreshold PSPs

Next, we investigated whether somatic depolarization can also enhance the propagation of dendritic spikes generated in a more physiological manner through synaptic stimulation of the perforant path (PP) inputs to the distal CA1 PN dendrites. We placed an extracellular stimulating electrode in the SLM of CA1 (at least 200 $\mu$m from the dendritic patch location), the distal dendritic site of the PP inputs, and applied either a single stimulating pulse to elicit a subthreshold postsynaptic potential (PSP) or a strong, brief high-frequency burst of stimuli to elicit a dendritic spike (four or five stimuli at 200 Hz; Fig. 4*A*).

Propagation of the subthreshold PSP evoked by a single PP stimulus or a subthreshold PSP-like signal evoked by dendritic current injection (Δ-EPSP) showed little dependence on somatic depolarization. Thus, the PSP amplitude at the soma was attenuated by a factor of 9.49 ± 1.67 at −70 mV and 8.96 ± 1.45 at −57.5 mV ($p = 0.94$, $n = 7$; Fig. 4*A*–*C*). In contrast, the propagation of a dendritic spike evoked by a brief train of synaptic stimuli (five stimuli at 200 Hz) was greatly enhanced by somatic depolarization in a manner similar to that observed when we evoked a dendritic spike through direct current injection (Fig. 1). Thus, the synaptically evoked spike amplitude attenuation at the soma was 33.4 ± 4.0 at −70 mV versus 9.8 ± 1.2 at −57.5 mV, $p = 0.015$, $n = 7$ (Fig. 4*A*,*F*,*G*). Moreover, with sufficient somatic depolarization, the synaptically evoked dendritic spike also led to burst firing of somatic APs.

The application of 4-AP (5 mM) caused a small but significant increase in the subthreshold PSP amplitude in both the dendrite and the soma (in both cases $p = 0.03$, $n = 7$; Fig. 4*A*,*D*). This change in amplitude may be because of presynaptic or postsynaptic effects or a combination of both (Migliore et al., 1999; Migliore, 2003; Palani et al., 2010). However 4-AP did not alter dendritic propagation of the subthreshold PSP, at either a somatic voltage of −70 or −57.5 mV (Fig. 4*B*,*D*; dendritic attenuation was 8.71 ± 1.34 at −70 mV and 8.44 ± 1.34 at −57.5 mV, $p = 0.57$, $n = 7$; Fig. 4*A*–*C*). In contrast, the propagation of the synaptically evoked dendritic spike was greatly enhanced by bath application of 4-AP at more negative but not depolarized somatic membrane potentials. In 4-AP, spike attenuation at −70 mV (10.53 ± 1.05, $n = 7$) was significantly less than that in control conditions (33.4 ± 4.0; $p = 0.0156$; Fig. 4*F*,*G*). In contrast, at −57.5 mV attenuation in 4-AP (9.02 ± 1.10) was similar to that in the absence of the drug (9.78 ± 1.19, $p = 0.109$, $n = 7$; Fig. 4*F*, *G*). 4-AP had no significant impact on the spike amplitude in the distal dendrite ($p = 0.08$, $n = 7$; Fig. 4*H*) nor did it alter PSP or dendritic spike duration (Fig. 4*E*,*I*), indicating that A-type $K^+$ channels are more important in regulating spike propagation along the apical dendrites in SR than spike generation in distal dendrites in SLM. This is consistent with previous pharmacological results (Cai et al., 2004) and the pattern of expression of Kv4.2 (Maletic-Savatic et al., 1995).

### Depolarization enhances dendritic spike firing and somatic bursting during paired activation of distal and proximal synaptic inputs

Paired activation of distal PP and proximal SC synaptic inputs can synergistically interact to generate firing of AP bursts and to induce Hebbian (Takahashi and Magee, 2009) and non-Hebbian forms of synaptic plasticity, including ITDP (Dudman et al., 2007; Basu et al., 2013, 2016). ITDP is most strongly induced when paired stimuli are delivered at 1 Hz for 90 s and when the distal input precedes the proximal input by 20 ms (−20 ms pairing interval,). During the standard 90-s induction protocol from a somatic potential of −70 mV, paired stimulation initially fails to elicit a dendritic spike. However, as the train of paired stimuli continues, the probability of spike firing increases, reflecting some unknown form of short-term intrinsic or synaptic plasticity. At a resting potential of −70 mV, the dendritic spikes fail to elicit somatic APs (Basu et al., 2016). This contrasts to the *in vivo* situation where dendritic plateau potentials trigger a burst of somatic AP output (Grienberger et al., 2014). As the CA1 PN somatic resting potential *in vivo* is depolarized by 10–15 mV

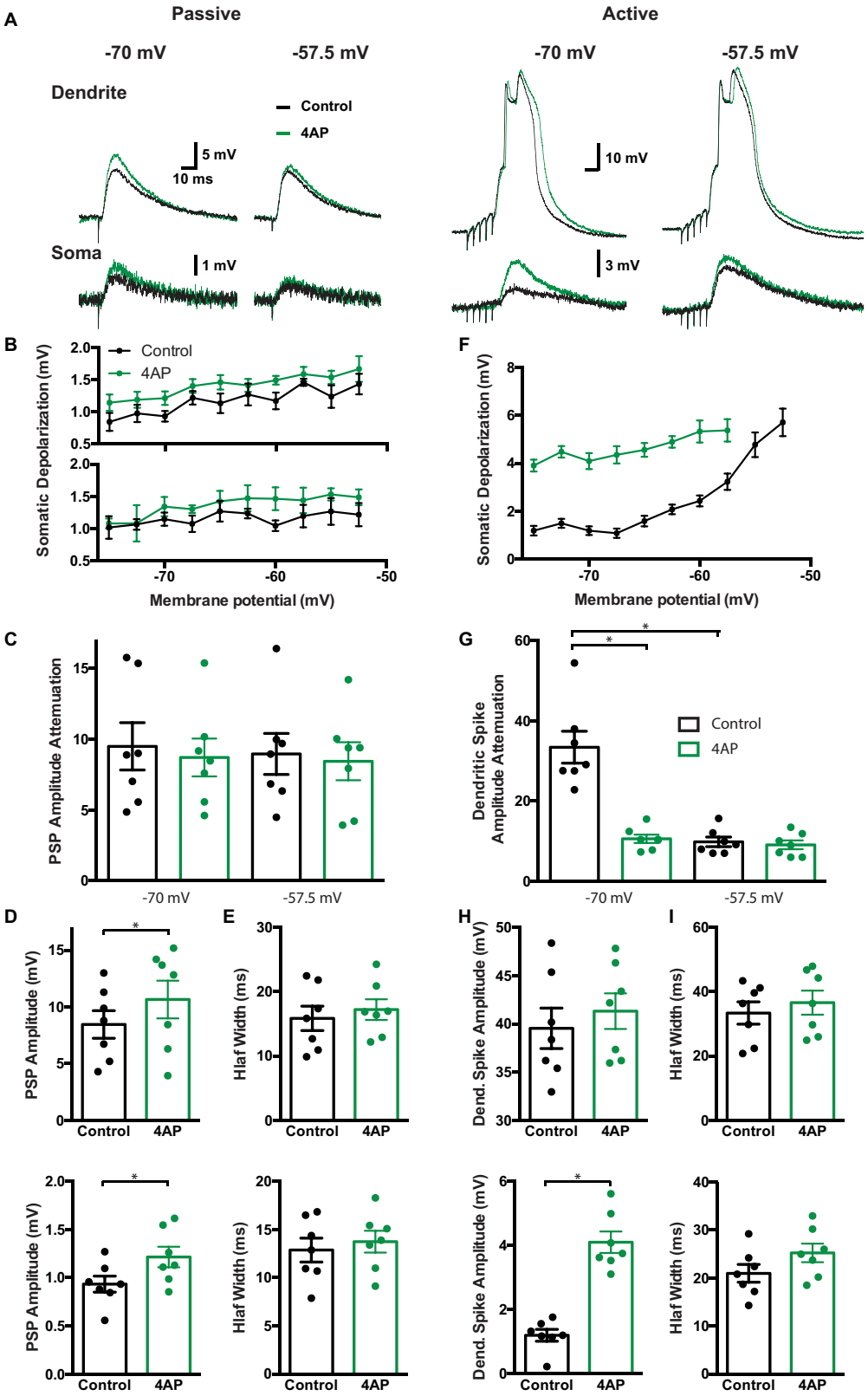


**Figure 4.** A-type $K^+$ channels affect active and passive signals differently. ***A***, Example traces of dendritic and somatic responses to single PP stimulation, which evokes a passively propagated PSP (left), and a train of five pulses of PP stimulation at 200 Hz, which evokes an actively propagating dendritic spike (right), when the soma is held at either −70 or −57.5 mV before (black) and after (green) application of 5 mM 4-AP. ***B***, Peak depolarization of the somatic membrane potential during a passively propagating PSP, evoked by extracellular stimulation (top) and a Δ-EPSP waveform (bottom), at varying somatic baseline potentials before (black) and after adding 4-AP (green). ***C***, The attenuation factor of passively propagating dendritic PSPs evoked by extracellular stimulation if the soma is held at −70 mV (left) or at −57.5 mV (right) before (black) or after (green) application of 4-AP. Data are paired as all conditions recorded consecutively in each of the patch-clamped cells. ***D***, Amplitude of passively propagating PSPs, evoked by single PP stimulation at the dendrite (top) and the soma (bottom) before (black) and after (green) bath application of 5 mM 4-AP. ***E***, Half width of passively propagating PSPs, evoked by single PP stimulation at the dendrite (top) and the soma (bottom) before (black) and after (green) bath application of 4-AP. ***F***, Peak depolarization of the somatic membrane potential during an actively propagating dendritic spike at varying somatic baseline potentials before (black) and after

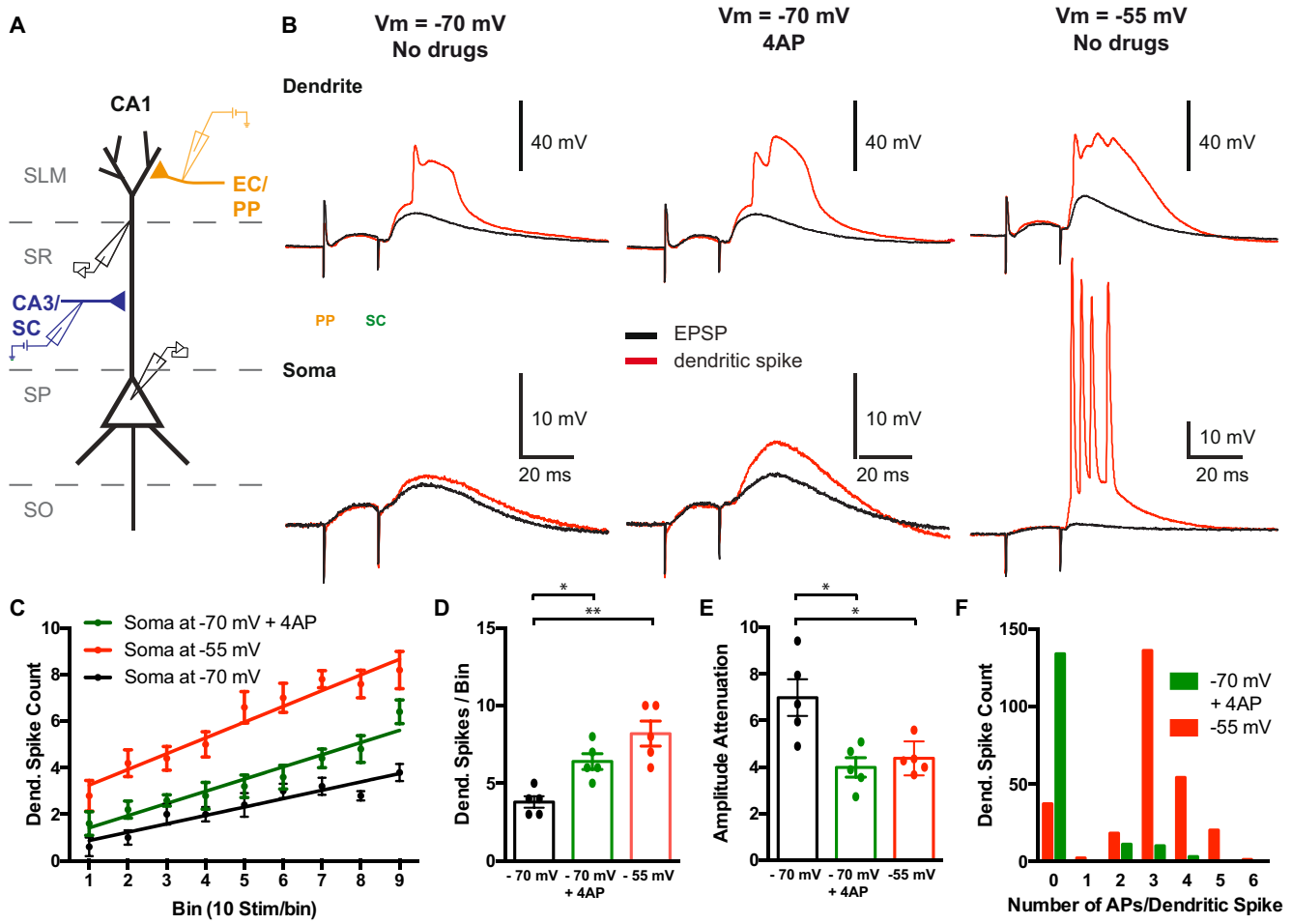


**Figure 5.** The impact of dendritic spikes at the soma during paired PP-SC stimulation. ***A***, Schematic of the experimental setup, showing the somatic and dendritic patch pipettes (black) as well as the PP (orange) and SC (blue) stimulating electrodes. ***B***, Example traces of the somatic (bottom) and dendritic (top) responses to ITDP induction stimuli for all three tested conditions [soma was held at −70 mV (left); 4-AP was present in the bath during induction (middle); soma was held at −55 mV during induction stimulation (right)]; black traces show examples of subthreshold PSPs, red traces show examples in which the SC stimulus elicited a dendritic spike. ***C***, Average number of dendritic spikes in 10-s bins during the induction period. The 90 paired stimuli were separated into nine bins of 10 stimuli each and the number of dendritic spikes in each bin was counted [black, soma was held at −70 mV; green, 4-AP (5 mM) was present in the bath during induction; red, soma was held at −55 mV during induction stimulation]. Straight lines show linear regression fits. ***D***, Dendritic spike count during the last 10 stimuli of the induction (black, soma was held at −70 mV; red, soma was held at −55 mV during induction stimulation; green, 4-AP was present in the bath during induction). ***E***, Attenuation of the somatic depolarization when a dendritic spike was elicited by the paired PP-SC stimulation (black, soma was held at −70 mV; green, 4-AP was present in the bath during induction; red, soma was held at −55 mV during induction stimulation). ***F***, Distribution of the number of somatic APs caused by dendritic spikes during paired PP-SC stimulation when 4-AP was present in the bath (green) or when the soma was depolarized to −55 mV during the induction period (red). $*p < 0.05$, $**p < 0.01$; Mann-Whitney test after Kruskal-Wallis test.

relative to that in *ex vivo* slices, we examined the influence of somatic depolarization on dendritic spike firing and propagation in response to paired distal and proximal stimuli at the −20-ms ITDP pairing interval.

We obtained dual apical dendritic and somatic whole-cell patch clamp recordings and either blocked A-type $K^+$ channels or manipulated the somatic membrane potential during the 90-s period of 1-Hz paired stimulation (Fig. 5*A*,*B*). To control for potential effects of the channel blockers or somatic depolarization on subthreshold PSP amplitude, we adjusted the strength of both the PP and SC stimulating currents to elicit approximately the same sized synaptic responses to the initial test stimuli and during the ITDP induction protocol (comparison of dendritic PP and SC PSPs from a holding potential of −70 mV in the presence and absence of 4-AP and from holding potential of −55 mV in absence of 4-AP using a Kruskal–Wallis test; PP PSPs, $p = 0.62$; SC PSPs, $p = 0.09$; $n = 5$).

As described above, with the membrane at −70 mV a 1-Hz train of paired stimuli of distal and proximal inputs elicited dendritic spikes that propagated poorly to the soma (Fig. 4*B*; Basu et al., 2016). Application of 4-AP at a resting potential of −70 mV or depolarization of the membrane to −55 mV enhanced the propagation of dendritic spikes elicited by paired synaptic stimuli (Fig. 5*E*). In addition, either depolarization or 4-AP increased the probability that a pair of stimuli would elicit a dendritic spike at various times during the train (Fig. 5*C*). More specifically, the rate of increase of dendritic spike firing throughout the time course of ITDP induction, measured as the slope of the linear regression (0.36 when the soma was held at −70 mV, $n = 5$), was

←

adding 4-AP (green). ***G***, Same as ***C*** but for actively propagating signals. ***H***, Amplitude of actively propagating dendritic spikes, evoked by high-frequency PP stimulation at the dendrite (top) and the soma (bottom) before (black) and after (green) bath application of 4-AP. ***I***, Half Width of actively propagating dendritic spikes, evoked by high-frequency PP stimulation at the dendrite (top) and the soma (bottom) before (black) and after (green) bath application of 4-AP. $*p < 0.05$; Wilcoxon test.

enhanced by both 4-AP (to 0.52, $p = 0.038$ compared with −70 mV with multiple comparison test, $n = 5$) and somatic depolarization to −55 mV (to 0.67; $p = 0.021$, compared with −70 mV with multiple comparison test, $n = 5$; Fig. 5*C*). With the membrane at −70 mV the number of dendritic spikes elicited by the last 10 paired stimuli of the train increased from 3.8 ± 0.4 in the absence of 4-AP to 6.4 ± 0.5 in the presence of 4-AP ($p = 0.079$). Depolarization to −55 mV in the absence of 4-AP caused an even larger increase in the number of dendritic spikes, to 8.2 ± 0.8 ($p = 0.016$ relative to −70 mV without 4-AP; Fig. 5*D*).

Of interest, when somatic APs were blocked by local application of TTX to the soma while the soma was depolarized to −55 mV, the number of dendritic spikes still increased significantly during the 90 s of paired stimulation (see below) and increased relative to dendritic spike firing at a somatic potential of −70 mV. Thus, the short-term plastic process that enhances dendritic spike firing during the train of paired stimuli does not require somatic AP firing but rather may be triggered by dendritic spiking alone. Moreover, as neither somatic depolarization nor 4-AP alters the local threshold in the dendrite for firing a dendritic spike in response to a single current injection (Tables 1, 2), the effect of 4-AP or somatic depolarization to enhance the probability of dendritic spike firing during the train of paired stimuli (relative to spike firing with the normal resting potential of −70 mV in the absence of 4-AP) likely reflects their action to enhance dendritic spike propagation.

Although the probability of dendritic spike firing increased progressively during the 90 s of paired stimulation with the resting membrane at −70 mV (Fig. 5*C*), the dendritic spikes were ineffective in eliciting a somatic AP. Of the 104 dendritic spikes elicited by synaptic pairing, only two triggered a somatic AP (1.9%, $n = 5$ cells). Moreover, in these two instances, the soma fired only one or two APs. Application of 4-AP or somatic depolarization greatly increased the probability that a dendritic spike would elicit one or more somatic APs. Thus, in the presence of 4-AP, 24 out of 158 dendritic spikes elicited a somatic AP (15.2%; $p = 0.0004$ with $\chi^2$ test relative to control, $n = 5$ cells). Moreover, when a dendritic spike was successful in activating the soma, it now triggered a burst of 2 or more spikes, with an average of 2.67 ± 0.14 somatic APs per dendritic spike. Depolarization to −55 mV was even more effective in triggering a burst of somatic actions potentials, with 231 out of 268 dendritic spikes elicited by paired stimulation evoking one or more somatic APs (86.2%, $p < 0.0001$ with $\chi^2$ test relative to control and 4-AP, $n = 5$ cells), with an average of 2.87 ± 0.08 APs per burst ($p < 0.0001$ with Mann–Whitney test relative to 4-AP; Fig. 5*F*).

At least two factors may contribute to the effect of somatic depolarization to enhance the firing of somatic APs in response to a dendritic spike elicited by paired stimulation. The first is the effect of somatic depolarization to enhance dendritic spike propagation. The second is the effect of somatic depolarization to bring the membrane closer to threshold. We believe that both factors are important as somatic spikes were never triggered by paired stimuli that failed to trigger a dendritic spike, even with the soma held at −55 mV. Additionally, 4-AP caused a significant increase in the amplitude of the somatic response to a dendritic spike (5.93 ± 0.53 to 9.39 ± 1.24 mV, $p < 0.05$ with Mann–Whitney test, $n = 5$; Fig. 5*E*), while not significantly changing somatic AP threshold (Table 2), indicating that the enhanced propagation of dendritic spikes itself leads to increased firing of somatic APs.

### Manipulations that enhance dendritic spiking enhance the induction of ITDP

Our finding that somatic depolarization enhanced dendritic spike firing during paired distal and proximal synaptic stimulation suggests that somatic resting potential may also regulate the induction or expression of ITDP. When the membrane was depolarized to −55 mV, the ITDP protocol induced a final level of potentiation to 312.4 ± 9.5% ($n = 5$) of its initial level, similar to that seen with the membrane held at −70 mV (297.2 ± 19.6%, $n = 7$; $p = 0.76$ relative to −55 mV). However, membrane depolarization greatly accelerated the time course of onset of potentiation. With the soma held at −70 mV, the ITDP induction protocol resulted in a slowly developing enhancement in the PSP amplitude over a period of 20 min, as previously described (Dudman et al., 2007; Basu et al., 2013, 2016), with the PSP increasing to only 138.5 ± 8.1% ($n = 7$) of its initial value 2 min after the end of the ITDP induction protocol. However, with the membrane held at −55 mV, the PSP increased to 225 ± 11.2% ($n = 5$) of its initial value at this time ($p = 0.0025$ relative to −70 mV; Fig. 6*A–E*). Application of 4-AP (with the membrane at −70 mV) also sped the onset of ITDP, with the PSP increased to 184.6 ± 14.5% ($p = 0.014$ relative to −70 mV with no 4-AP, $n = 5$) after 2 min (Fig. 6*E*), with no enhancement in ITDP magnitude after 20 min (PSP increased to 308.5 ± 32.7%, $p = 0.88$, $n = 5$). Importantly, membrane depolarization did not alter the tuning of ITDP induction to the −20-ms pairing interval ($p = 0.0019$ with Kruskal–Wallis test, $n = 5$/time interval; Fig. 6*F*). This characteristic input timing dependence indicates that the plasticity mechanism enhanced by 4-AP or somatic depolarization is indeed related to ITDP, rather than some other form of long-term plasticity, such as LTP or spike-timing-dependent plasticity (STDP).

If dendritic spikes are critical for the induction of ITDP, we predicted that it might be possible to induce ITDP with fewer than 90 paired stimuli when dendritic spiking is enhanced. We therefore examined the effect of varying the number of paired stimuli on the magnitude of ITDP with the soma held at −70 mV in the absence and presence of 4-AP or with the soma held at −55 mV (no 4-AP). At a holding potential of −70 mV (in the absence of 4-AP), 80 stimulus pairs were required to produce a significant potentiation of the PSP measured 20 min after the induction protocol ($p = 0.011$ with Mann–Whitney test after Kruskal–Wallis test), with 90 stimulus pairs required to double the size of the PSP (an increase of 197.2 ± 19.6%, $n = 7$; Fig. 7*A*, *B*). However, in the presence of 4-AP only 50 stimulus pairs were required to produce a significant potentiation ($p = 0.039$ with Mann–Whitney test after Kruskal–Wallis test), with 60 stimuli sufficient to cause a doubling of the PSP (PSP increase to 207.5 ± 27.3% of its initial level, $n = 5$; Fig. 7*A*,*C*). Fifty stimulus pairs were also sufficient to cause a significant increase in the PSP in the presence of the Kv4.2/3 channel blocker phrixotoxin-2 (the SC response increased to 200.4 ± 17.8% after 20 min, $p = 0.048$, $n = 4$; Fig. 7*A*). The effect of somatic membrane depolarization to −55 mV was even more pronounced, with a significant potentiation being produced after only 20 stimuli ($p = 0.031$ with Mann–Whitney test after Kruskal–Wallis test), and 40 stimuli sufficient to more than double the PSP (223.8 ± 22.2%, $n = 5$; Fig. 7*A*,*D*).

We observed a strong correlation between the number of dendritic spikes during the induction period and ITDP expression, especially over the range of 15–30 dendritic spikes. This was observed either when the soma was depolarized to −55 mV during ITDP induction (nonparametric Spearman correlation

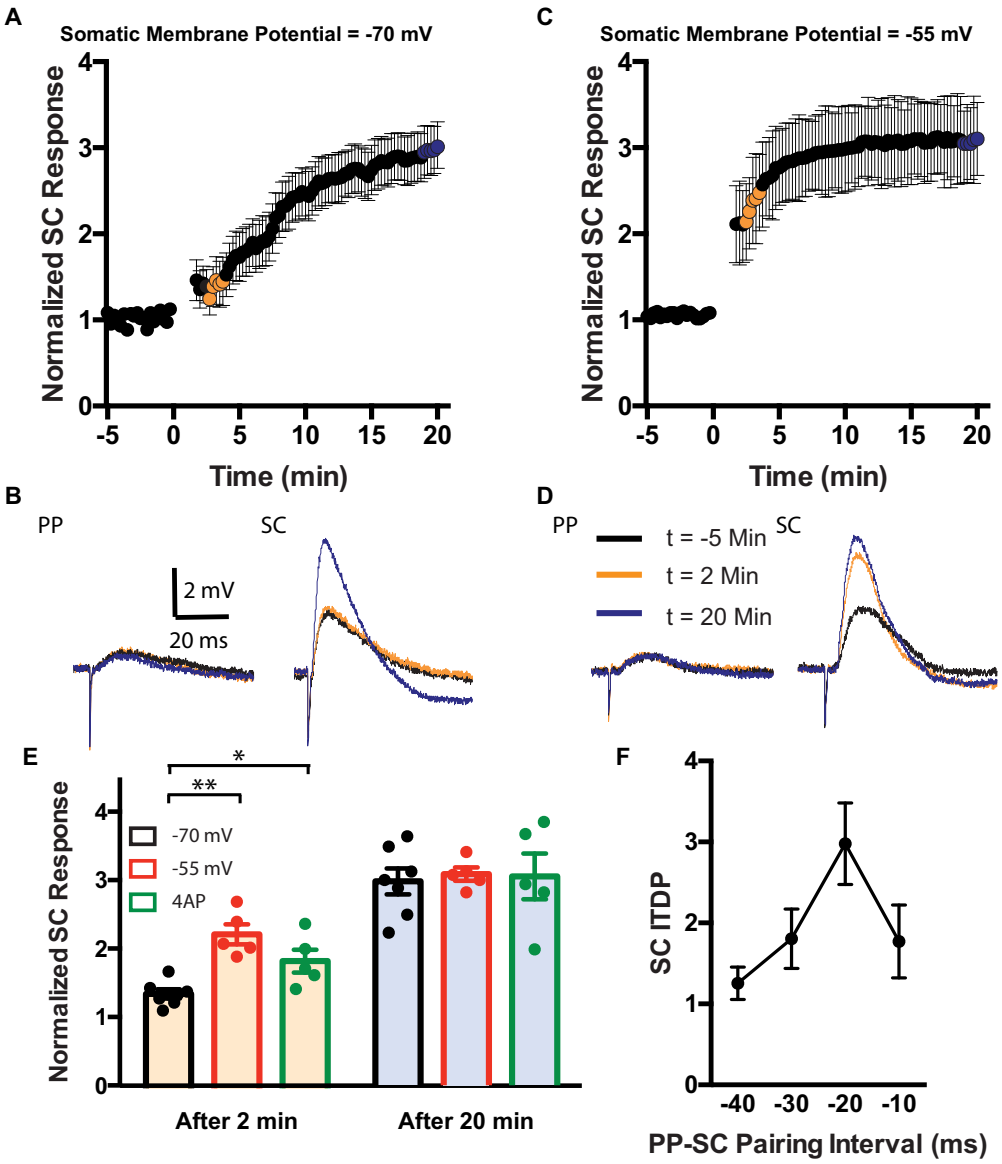


**Figure 6.** Manipulating the somatic membrane potential affects onset of ITDP expression. ***A***, Somatic PSP response to SC stimulation before and after ITDP induction, normalized to the response before induction (orange and blue symbols represent the time points that were used for averages in later panels). ***B***, Example traces of PSPs in response to PP (left) and SC stimulation before (black) and 2 min (orange) and 20 min (blue) after ITDP induction. ***C***, ***D***, Same as ***A***, ***B***, respectively, except that in this case, the soma was depolarized to −55 mV during the induction stimuli. ***E***, Comparison between the normalized response to SC stimulation 2 min (orange filled bars) and 20 min (blue filled bars) after ITDP induction at a membrane potential of −70 mV (black) or −55 mV (red) or if 4-AP was bath applied during ITDP induction (green). ***F***, Normalized response to SC stimulation 20 min after ITDP induction at a membrane potential of −55 mV at varying PP-SC intervals during the induction. *$p < 0.05$, **$p < 0.01$; Mann-Whitney test after Kruskal-Wallis test.

factor r = 0.66, $p = 0.009$ in this range, $n = 15$ cells; Fig. 7*E*) or when 4-AP was present in the bath (r = 0.78, $p = 0.002$, $n = 14$ cells; Fig. 7*F*). This correlation supports the view that dendritic spike firing during the paired synaptic stimulation plays an important role in the induction of ITDP. For technical reasons, most of the ITDP experiments were performed with only somatic recordings. As a result, we could not evaluate the correlation under control conditions, as dendritic spikes were only detectable in somatic recordings under conditions that favored spike propagation (Fig. 5*B*).

Given the correlation between the number of dendritic spikes and ITDP, the effect of somatic depolarization to enhance the induction of ITDP is likely to result, at least in part, from the increased firing of dendritic spikes. Might the enhancement in dendritic spike propagation to the soma also contribute to the enhancement in induction of ITDP? To address this question, we plotted the onset of ITDP with the soma at either −70 or −50 mV as a function of the number of dendritic spikes observed during the induction protocol (Fig. 7*G*). We found that the onset of ITDP elicited by the same number of dendritic spikes was significantly greater when the membrane was depolarized. A linear fit to the ITDP versus spike number relation yielded y intercept values of $-0.20 \pm 0.43$ at −70 mV and $0.35 \pm 0.50$ at −55 mV [$p = 0.0005$ with linear regression analysis, $n = 7$ (−70 mV) and 5 (−55 mV); Fig. 7*G*]. This result suggests that depolarization can enhance ITDP onset independently of enhancing dendritic spike firing, consistent with a role for DEDSP enhanced dendritic spike propagation. This effect of depolarization was not visible in the SC response 20 min after ITDP induction (data not shown), which is consistent with our earlier finding that after 20 min, the increase in the SC response reaches a plateau level (Fig. 6).

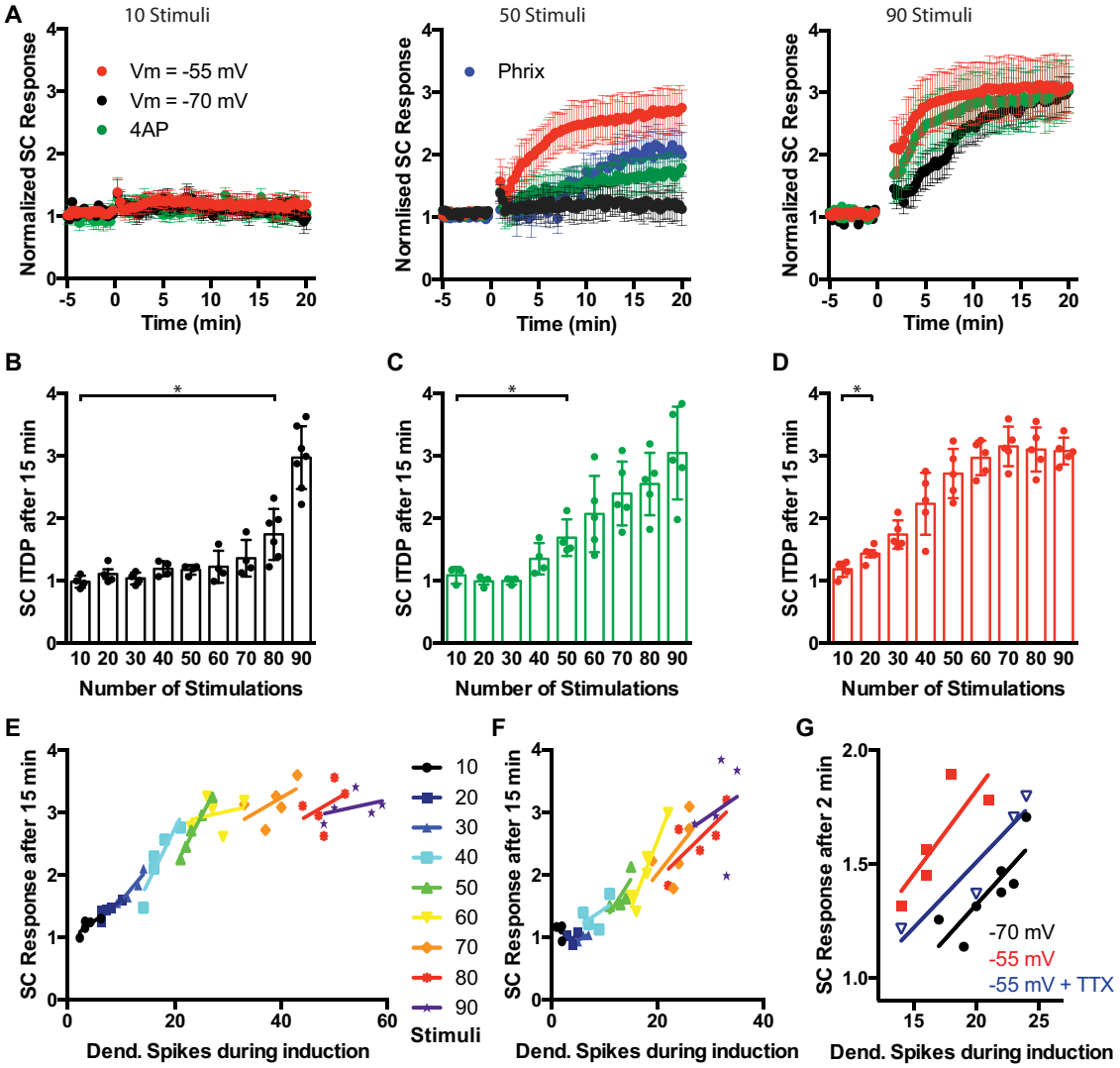


**Figure 7.** Somatic membrane depolarization or block of A-type $K^+$ channels enhances the efficiency of ITDP induction. ***A***, Change of the somatic PSP response to SC stimulation after ITDP induction, if the number of induction stimulus pairs is reduced to 10 (left), 50 (middle), or is kept at the usual 90 stimuli (right), colors indicate the condition of the cell during induction (black, soma was held at −70 mV; green, 4-AP was present in the bath during induction; red, soma was held at −55 mV during induction stimulation; blue, 500 nM phrixotoxin-2 was present in the bath during induction with 50 stimuli). ***B***, Average change in the somatic response to SC stimulation 20 min after ITDP induction, if the number of induction stimulus pairs is incrementally decreased from 90 pairs to 10 in steps of 10 and soma was held at −70 mV during induction. ***C***, Same as ***B*** but in the case that 4-AP was bath applied during ITDP induction. ***D***, Same as ***B*** but in the case that the soma was held at −55 mV during ITDP induction. ***E***, Correlation between number of dendritic spikes during a given ITDP induction protocol and the increase in the SC response after 15 min when the soma is depolarized to −55 mV. ***F***, Same as ***E*** but when the soma is held at −70 mV and 4-AP is present in the bath. For ***E*** and ***F***, each point is an individual cell. ***G***, Correlation between the total number of dendritic spikes during ITDP induction and the SC response 2 min after ITDP induction (normalized to PSP before induction) within a stimulus range that yielded a total of 13–27 dendritic spikes when the cell soma was held at −70 mV (black), or at −55 mV under control conditions (red) or during somatic application of TTX (blue). *$p < 0.05$; Mann-Whitney test after Kruskal-Wallis test.

As the dendritic spikes can trigger AP output with the membrane held at −55 mV but not with the membrane at −70 mV, we examined whether the enhanced induction of ITDP from the more positive somatic potential was a result of the enhanced firing of somatic spikes. We locally applied TTX to the soma during paired stimulation to block the firing of somatic APs without altering dendritic spikes or SC PSPs (Fig. 8*A–C*). Under these conditions, somatic depolarization was still able to enhance the induction of ITDP, which displayed a characteristic rapid onset (Fig. 8*D*) and ability to be induced with only 50 paired stimuli (Fig. 8*E*). Similarly, even in the presence of TTX, somatic depolarization enhanced the relation between ITDP at 2 min and the number of dendritic spikes during induction (y intercept $0.34 \pm 0.15$, $p = 0.0058$ relative to −70 mV with linear regression analysis, $n = 4$; Fig. 7*G*). These results clearly indicate that an increase in the efficacy of dendritic spike propagation and/or generation is sufficient to increase the efficacy of ITDP induction. However, as the rate of development of ITDP with the membrane at −55 mV is somewhat greater in the absence of TTX than in the presence of TTX, increased somatic spike firing is also likely to be important.

### Dendritic spikes are necessary and sufficient to induce ITDP in conjunction with SC stimulation

To probe more directly the importance of dendritic spikes, we determined whether they were sufficient and/or necessary to induce ITDP. We conducted dual patch clamp recordings at the soma and distal apical dendrite of CA1 PNs as before. However, instead of the normal ITDP induction protocol, we omitted the PP stimulus and administered 90 SC stimuli at a frequency of 1 Hz, either alone or paired with a dendritic spike elicited by

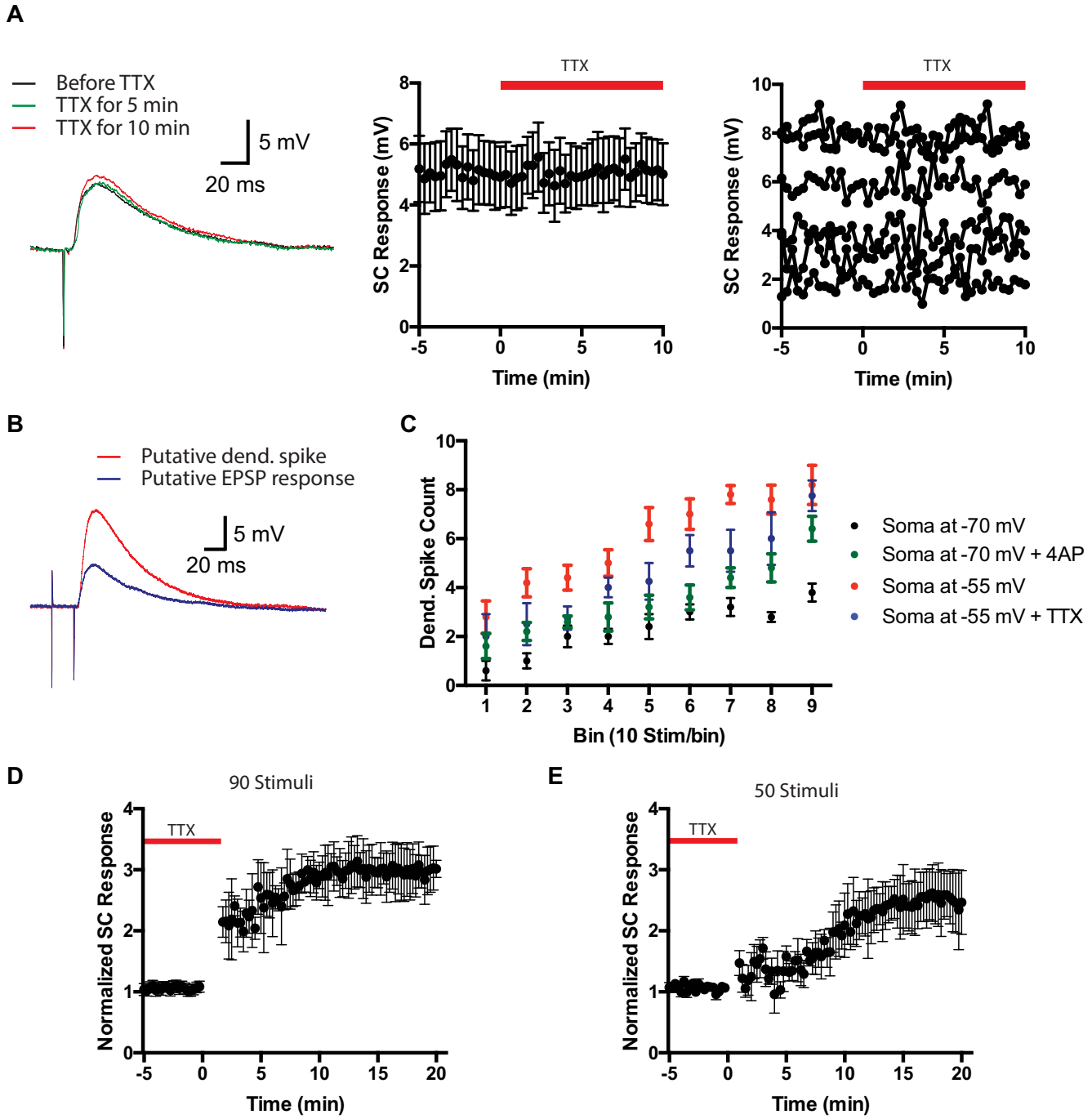


**Figure 8.** Depolarization of the somatic membrane during ITDP induction in the presence of TTX. ***A***, Left, Example traces of PSPs in response to a single SC stimulus before (black), after 5 min (green), and after 10 min (red) of TTX, applied to the soma through a local puffing pipette. Middle, The average response to SC stimulation during local somatic TTX application remains unchanged ($n = 6$). Right, Same as the middle graph but showing the responses of the individual cells. ***B***, Example traces of the somatic response to ITDP induction stimulation in those cases where a dendritic spike occurred (red) or did not (blue). The cell soma was depolarized to −55 mV, and TTX was applied to the soma (compare to Fig. 4*B*). ***C***, Average occurrence of dendritic spikes during the induction period. The 90 paired stimuli were separated into nine bins of 10 stimuli each and the number of dendritic spikes in each bin was counted (black, soma was held at −70 mV; red, soma was held at −55 mV during induction stimulation; green, 4-AP was present in the bath during induction; blue, TTX was applied to the soma and the soma was held at −55 mV during induction stimulation). ***D***, Change of the somatic PSP response to SC stimulation after 50 ITDP induction stimuli when TTX was applied to the soma and the soma was depolarized to −55 mV during induction ($n = 4$). ***E***, Same as ***D*** but after 90 induction stimuli ($n = 3$).

direct dendritic current injection. The 90 SC stimuli alone caused no significant increase in the PSP in the following 20 min (113.5 ± 5.7%, $p = 0.65$, $n = 8$; Fig. 9*A–D*). Next, we examined the effect, in the same cell, of pairing each of the 90 SC stimuli with the injection of a depolarizing 2-ms, 400-pA current step into the dendrite 3–5 ms after the SC stimulus. We chose this delay as it was within the time window in which we observed the onset of the dendritic spike during paired PP-SC stimulation at the −20-ms interval (Fig. 5*B*, upper traces) and roughly coincided with the peak of the SC PSP measured in the dendrite. The pairing of SC synaptic stimulation and distal dendritic current injection evoked a dendritic spike with a high probability (89.6%, $n = 450$ stimuli in 5 cells). Importantly, the pairing also induced a large ITDP-like enhancement in the SC PSP measured in the distal

dendrite, which progressively increased in amplitude within the following 20 min to 194.8 ± 18.0% of its value before pairing (from 6.23 ± 0.76 mV before pairing to 11.21 ± 0.84 mV after pairing, $p = 0.008$, $n = 8$; Fig. 9*A–D*).

Does the potentiation induced by paired SC stimulation and dendritic spiking reflect the same plasticity mechanism as ITDP induced by paired synaptic stimulation? ITDP largely results from the long-term-depression of the component of the feedforward IPSP evoked by SC stimulation (iLTD) that is mediated by cholecystokinin-positive ($CCK^+$) interneurons (accounting for ~75% of the potentiation of the PSP), with a smaller component caused by LTP of the EPSP (eLTP; accounting for ~25% of the potentiation; Basu et al., 2013). To determine whether pairing of SC stimulation with dendritic spiking also suppressed the IPSP, we assessed the extent of inhibition by applying blockers of $GABA_A$ (2 μM SR95531) and $GABA_B$ (1 μM CGP55845) receptors on the PSP amplitude before and after induction of plasticity. Normally, the application of the GABA receptor antagonists produced a nearly 3-fold increase in the peak depolarization during the SC PSP because of blockade of the rapid feedforward IPSP (peak SC PSP increased to 282.6 ± 40.9% of initial value, $p = 0.031$, $n = 6$; Fig. 9*E*). However, 20 min following the induction of ITDP with paired synaptic stimulation, the blockers increased the PSP to only 133.0 ± 14.2% of its value relative to control ($p = 0.125$, $n = 4$; Fig. 9*L*), indicating a pronounced decrease in feedforward inhibition. We observed a similar loss of sensitivity to $GABA_A$ and $GABA_B$ receptor blockade (SR95531 and CGP55845) 20 min after pairing SC stimulation with dendritic spikes, with the blockers increasing the PSP to only 114.3 ± 2.5% of control (PSP increased from 10.78 ± 1.29 to 12.35 ± 1.60 mV, $p = 0.13$, $n = 4$; Fig. 9*F*).

To further confirm that the plasticity induced by pairing SC stimulation with dendritic spike firing was related to ITDP, we applied the induction protocol with inhibition continuously blocked (using SR95531 and CGP55845). This largely eliminated the enhancement of the PSP, with only a small residual potentiation (127.5 ± 6.8%, $n = 4$), which likely reflects the small component of eLTP recruited by ITDP induction (Fig. 9*G*). These results thus support the view that the plasticity induced by pairing SC stimulation with dendritic spiking largely resulted from ITDP. In contrast, if the pairing protocol induced conventional Hebbian LTP or STDP, it should have been greatly enhanced with inhibition blocked (because of increased postsynaptic depolarization).

As a third approach to determine the nature of the plasticity mechanism, we examined the effects of bath application of the endocannabinoid CB1 receptor blocker AM251 (2 μM) during the ITDP induction protocol. Because the iLTD component of ITDP results from the activation of CB1 receptors on presynaptic terminals of $CCK^+$ interneurons, AM251 blocks the majority of ITDP induced by paired synaptic stimulation (Basu et al., 2013). Consistent with these results, application of AM251 also greatly reduced the synaptic potentiation produced by pairing dendritic spikes with SC stimulation (144.3 ± 11.9%, $n = 5$, which is significantly less than the potentiation in the absence of the blocker seen above; $p = 0.0062$), with the residual potentiation likely resulting from eLTP (Fig. 9*H*).

We thus conclude that dendritic spikes in conjunction with SC stimulation are sufficient to induce ITDP. But are dendritic spikes necessary? Can ITDP be induced during paired distal and proximal synaptic stimulation if dendritic spikes are prevented? Addressing this question is complicated by the fact that pharmacological blockade of active dendritic events would also compromise synaptic transmission, which is essential for ITDP induction. We therefore suppressed the generation of dendritic spikes electrically by using an online computer-controlled program to inject negative current into the dendrite to prevent dendritic spiking whenever the membrane depolarized to the dendritic spike threshold. This prevented dendritic spikes from occurring while keeping interference with summation of distal and proximal PSPs at a minimum, as long as they remain below the threshold for negative current injection (Fig. 9*I*, dotted line). Prevention of dendritic spikes in this manner almost fully suppressed ITDP evoked by the standard paired synaptic stimulation protocol. Twenty min after delivering the induction protocol with dendritic spikes suppressed, the SC-evoked PSP was increased to only 126.5 ± 7% of its initial value, compared with the 274.3 ± 34.2% increase under normal condition ($p < 0.05$ with Mann–Whitney test, $n = 4$; Fig. 9*I–K*).

To assess the extent of inhibition when the ITDP induction protocol was delivered with dendritic spiking suppressed, we applied $GABA_A$ and $GABA_B$ receptor antagonists (SR95531 and CGP55845) 20 min after paired stimulation. After pairing, the blockers still caused a large increase in the net SC PSP amplitude (to 310.8 ± 40.0%, $p < 0.0001$, $n = 4$; Fig. 9*I–K*), similar to their effect under baseline conditions. Thus, the prevention of dendritic spiking suppressed the induction of iLTD. In contrast, when we allowed dendritic spikes to occur normally during the ITDP induction protocol, we observed an increase of the SC response to 252.9 ± 34.1% of baseline ($p = 0.045$, $n = 4$), and subsequent application of SR95531 and CGP55845 caused only a slight, statistically insignificant increase in PSP amplitude (325.1 ± 32.6% from baseline but only 133.0 ± 14.2% from the post-ITDP SC response, $p = 0.125$, $n = 4$; Fig. 9*L*), consistent with previous results showing that ITDP largely suppresses feedforward inhibition (Basu et al., 2013). Together, these results indicate that dendritic spikes are both necessary and, in conjunction with SC stimulation, sufficient to induce ITDP.

## Discussion

Here, we report that the propagation efficacy of dendritic spikes generated in distal CA1 dendrites is powerfully controlled by the somatic membrane potential. As a result of the effect of somatic depolarization to enhance dendritic spike propagation, the level of membrane polarization at the soma and proximal dendrite can regulate whether distal synaptic input that is strong enough to trigger a local dendritic spike will remain confined to the distal dendrite or will have a more powerful impact on signal integration and AP output at the soma. In this way, DEDSP provides a powerful means by which synaptic input to one dendritic compartment can influence the efficacy of input to a distinct and spatially remote compartment.

Our results implicate dendritic A-type $K^+$ channels as an important mechanism contributing to DEDSP. In *ex vivo* slices, neurons are relatively isolated from their surrounding network and synaptic input is sparse, so the resting membrane potential of CA1 pyramidal cells is stable and fairly negative, around −70 mV (an average of −68.9 ± 0.8 mV in these experiments; see Table 1). At this low membrane potential, A-type $K^+$ channels will be in a fully available state with little resting inactivation (Hoffman et al., 1997). As a result, the channels will be able to conduct a large repolarizing $K^+$ current in response to a subsequent depolarization. Thus, as a dendritic spike

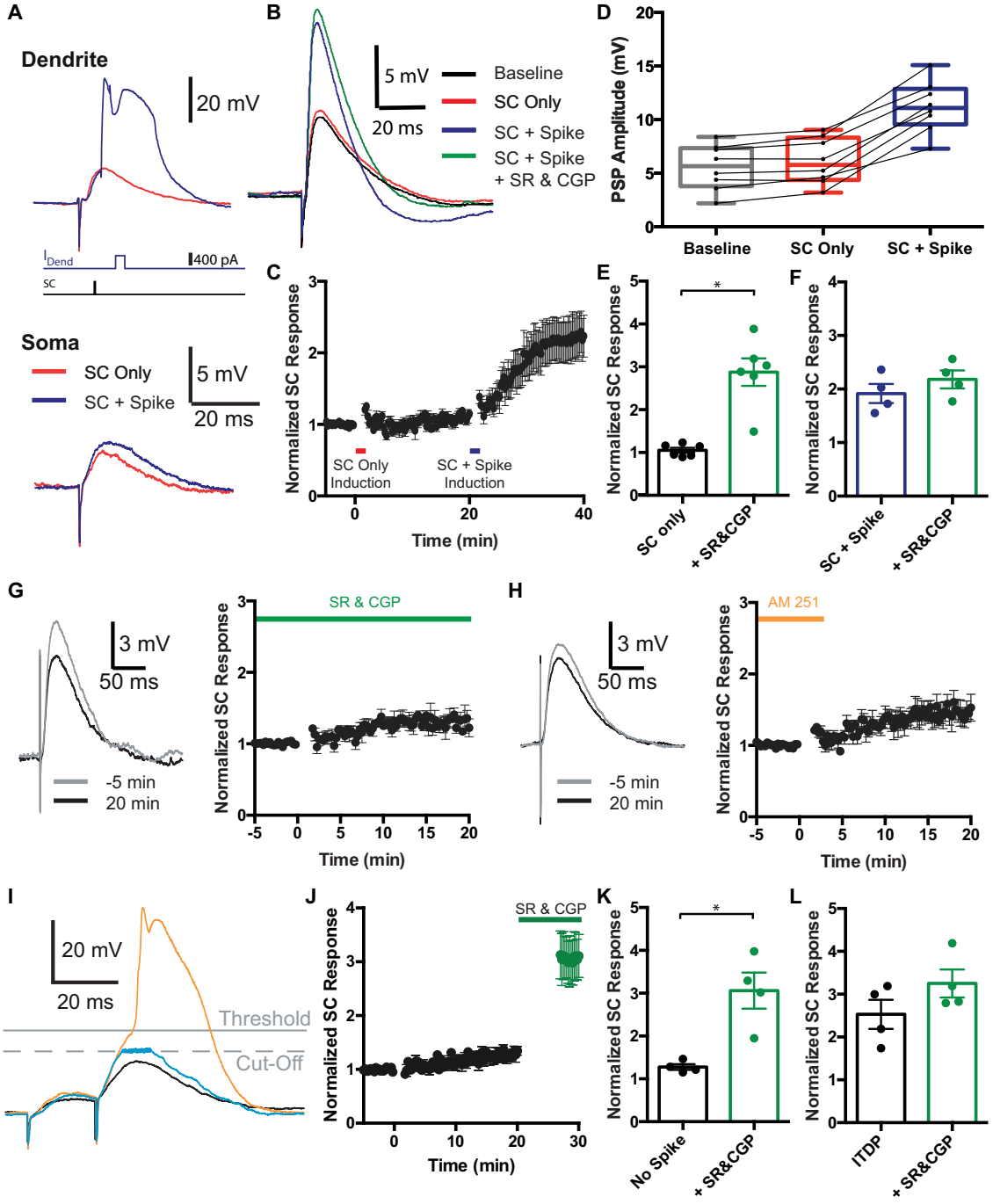


**Figure 9.** Dendritic spikes are sufficient and likely necessary for ITDP induction. ***A–D***, Pairing SC stimulation with a distal dendritic spike enhances the SC PSP, similar to ITDP. ***A***, Example traces of a modified ITDP induction protocol, where a SC stimulus is either paired with dendritic current injection sufficient to elicit a dendritic spike (blue) or is not paired with a dendritic spike (red). Top, Dendritic patch-clamp recording. Bottom, Somatic recording. ***B***, The SC PSP of the same cell before any stimulation (black), 20 min after 90 single SC stimuli were administered at 1 Hz (red), 20 min after 90 SC stimuli were combined with dendritic current injection to elicit dendritic spikes at 1 Hz (blue) and after subsequent bath application of 2 $\mu$M SR95531 and 1 $\mu$M CGP55845 (green). ***C***, Time course of the change in the SC PSP over the course of the experiment; the bars indicate the time of the 1-Hz SC stimulation first without (red) and then with (blue) dendritic current injection. ***D***, Summary of the SC PSP amplitude before and after the two stimulation modes described above; dots indicate single data points ($n = 8$). ***E–H***, Pairing SC stimulation and dendritic spike suppresses IPSP through CB1 receptor activation, similar to ITDP. ***E***, Average SC PSP amplitude 20 min after SC stimulation only, before (black) and after (green) application of SR95531 and CGP55845 ($n = 6$). GABA receptor antagonists increase the PSP because of blockade of IPSP. ***F***, Average SC PSP amplitude 20 min after combined SC stimulation and dendritic current injection before (blue) and after (green) bath application of SR95531 and CGP55845 in a subset of cells ($n = 4$). GABA receptor antagonists fail to alter PSP, consistent with view that paired SC+dendritic spikes induces ITDP, resulting in suppression of IPSP. ***G***, Change in SC PSP response after inducing ITDP with 90 SC stimuli at 1 Hz, each one combined with dendritic current injection to elicit dendritic spikes in the presence of 2 $\mu$M SR95531 and 1 $\mu$M CGP55845; green bar indicates the time at which SR95531 and CGP55845 are present in the bath ($n = 4$). GABA receptor antagonists reduced effect of pairing to enhance the PSP, consistent with view that PSP enhancement, like ITDP, is because of suppression of IPSP. ***H***, Change in SC PSP response after inducing ITDP with 90 SC stimuli at 1 Hz, each one combined with dendritic current injection to elicit dendritic spikes with 2 $\mu$M AM251 present in bath (orange bar) during the stimulation ($n = 5$). Reduction in effect of SC+dendritic spikes to enhance PSP indicates dependence on CB1 receptors, similar to ITDP. ***I–L***, Suppressing dendritic spikes during ITDP synaptic pairing protocol inhibits induction of ITDP and the reduction in IPSP. ***I***, Example traces of the dendritic voltage signal during ITDP induction showing effect of hyperpolarizing current during suprathreshold events. Black, A PSP that does not reach dendritic spike threshold did not trigger current injection. Orange, A PSP that reached dendritic spike threshold without delivery of a

propagates actively from the distal dendrites toward the soma, these channels will rapidly activate and reduce the efficacy of spike propagation. However, if the cell is maintained in a slightly depolarized state before dendritic spike firing, a significant fraction of A-type $K^+$ channels in the proximal dendrites will be inactivated, decreasing the amount of outward $K^+$ current activated by a dendritic spike and, thereby, permitting efficient active dendritic spike propagation. Our experimental results corroborate previous experimental results on the effect of membrane voltage to enhance the propagation of dendritic $Na^+$ spikes along the apical dendrites of rat CA1 PNs (Gasparini et al., 2004). In addition, we find that resting potential powerfully regulates the calcium-dependent long-lasting dendritic spike, as the effect of somatic membrane potential on propagation remains in the presence of TTX (Figs. 1, 2). The results in this study are also consistent with experimental results showing that A-type $K^+$ channels limit back propagation of APs into the dendrite (Hoffman et al., 1997; Magee and Carruth, 1999). Furthermore, our computational model shows how fast activating A-type $K^+$ channels in the apical trunk impede the propagation of the dendritic calcium spike, thereby reducing the resulting depolarization in the soma.

Our experimental results, supported by our model, further indicate that the propagation of passive signals, such as single PSPs that did not reach the threshold for dendritic spiking, was not affected significantly by A-type $K^+$ channels in the apical dendritic trunk. This may be because of the low amplitude of these signals, which may not cause sufficient A-type $K^+$ channel activation to affect PSP amplitude attenuation at the soma.

A study by Hsu et al. (2018) has shown that the excitatory somatic response to a brief high-frequency train of weak subthreshold distal EPSPs that fail to elicit a dendritic spike can also be amplified by somatic depolarization. However, this mechanism does not involve enhanced dendritic propagation but rather results from a local boosting at the soma as a result of activation of a perisomatic persistent voltage-gated $Na^+$ current (Hsu et al., 2018). Interestingly, Hsu and colleagues observed little effect of persistent $Na^+$ current on single subthreshold EPSPs or actively propagating dendritic plateau potentials, similar to our results. Together, the report of Hsu and colleagues and our findings indicate that there are distinct activity-dependent mechanisms for enhancing the influence of distal PP inputs on CA1 PN output depending on the dynamics and strength of that input.

In addition to enhancing forward propagation of distally-generated dendritic spikes, we find that when the soma is in a more depolarized state, dendritic excitability in response to back-propagating APs is increased (T. Bock and S. A. Siegelbaum, unpublished observations). This effect is consistent with the known role of A-type $K^+$ channels to limit bAP propagation (Hoffman et al., 1997) and the finding that subthreshold membrane potential changes modulate bAP propagation *in vivo* (Waters and Helmchen, 2004). This would suggest that somatic membrane potential not only determines the impact of dendritic spikes on the soma but also regulates the efficacy of their initiation in response to somatic APs.

Our findings of DEDSP in acute hippocampal slices may help explain the efficient triggering of complex spikes when an animal occupies a PN's place field. *In vivo*, CA1 PNs receive a constant barrage of background synaptic inputs to their somato-dendritic compartment, leading to a more depolarized resting potential (around −60 mV) compared with the resting potential in acute slices (−70 mV; Harvey et al., 2009; Epsztein et al., 2011; Lee et al., 2012; Grienberger et al., 2014; Bittner et al., 2015; Hulse et al., 2016). Moreover, *in vivo* recordings have shown a ramping of spike firing as an animal enters its place field (Mehta et al., 2000) that is associated with a depolarizing ramp potential (Harvey et al., 2009), which may represent a combination of subthreshold EPSPs arising from inputs to basal or proximal apical dendrites and dendritic spikes that poorly propagate to the soma. As the resting potential depolarizes during the ramp, A-type $K^+$ channel inactivation will increase progressively. Thus, place field membrane potential dynamics are ideally suited to enhance dendritic spike propagation and the firing of complex spikes.

DEDSP also provides a mechanism to explain recent *in vivo* findings that somatic depolarization through direct current injection can further enhance the frequency of complex spike firing (Grienberger et al., 2014) and lead to the appearance of *de novo* place field activity in a formerly silent CA1 neuron (Lee et al., 2012; Bittner et al., 2015; Zhao et al., 2022). As we found that depolarization does not enhance propagation of subthreshold EPSPs, the ability of somatic depolarization to reveal the presence of subthreshold place field events suggests that these events likely result from distal dendritic spikes that are unpaired with proximal synaptic events. The coincidence of distal dendritic spikes with large somatic depolarization, either through direct somatic current injection or strong proximal synaptic input, triggers the firing of a long-lasting dendritic plateau potential (Bittner et al., 2015), which results in a stable place field activity that outlasts the somatic depolarization, presumably through the induction of a form of synaptic plasticity (Bittner et al., 2017).

Our results further identify the importance of dendritic spikes for the induction of one form of synaptic plasticity, ITDP. Thus, we both confirm that the ITDP induction protocol is able to trigger the firing of dendritic spikes (Basu et al., 2016) and now provide evidence that dendritic spikes are sufficient to induce ITDP when paired with weak SC stimulation (Fig. 9*A–D*). Our data also suggest that dendritic spikes may be necessary for ITDP induction since we found that prevention of dendritic spike firing by applying hyperpolarizing dendritic current injections suppressed the induction of ITDP (Fig. 9*I–L*). Although we only injected hyperpolarizing current steps on detection of a suprathreshold dendritic event, and so we left all subthreshold PSPs intact, we cannot rule out the possibility that the suppression of ITDP was because of the blockade of the subset of very large, suprathreshold PSPs, rather than because of block of the spikes themselves. Our study further reveals a marked influence of somatic membrane potential on the efficacy of ITDP induction. Thus, depolarization of the soma from its normal resting potential of −70 mV observed in acute slices to −55 mV, a value attained *in vivo*, decreases the number of synaptic pairing events required to produce a significant potentiation by a factor of 4 (from 80 to 20). This likely overestimates the minimum number of pairing events required to induce ITDP because the somatic depolarization achieved by current injection through a patch electrode will decrement in the dendrite as a function of distance

←

hyperpolarizing current step. Light blue, A PSP that reached dendritic spike threshold with delivery of a hyperpolarizing current step, preventing firing of a dendritic spike. ***J***, Time course of SC PSP amplitude when dendritic spikes are electrically blocked during ITDP induction. The green data points indicate measurements after bath application of SR95531 and CGP55845, indicating presence of a large IPSP. ***K***, SC PSP amplitude before (black) and after (green) bath application of SR95531 and CGP55845 when dendritic spikes were electrically prevented during the ITDP protocol, indicating large IPSP. ***L***, Same as ***I*** when dendritic spikes were allowed to fire during ITDP induction, indicating loss of IPSP. $^*p < 0.05$; Mann-Whitney test.

from the soma. A more uniform depolarization of the entire somato-dendritic compartment, as achieved under physiological conditions, may enable ITDP induction with even fewer paired events.

Somatic depolarization is likely to enhance ITDP through several mechanisms. First, we find that somatic depolarization enhances the ability of the dendritic spikes to trigger a somatic AP, which also increases the firing of bAPs. As bAPs can broaden the dendritic spike (Larkum et al., 1999), they will enhance $Ca^{2+}$ influx, which could help promote ITDP. However, since we find that somatic depolarization significantly enhances ITDP even when somatic APs and bAPs are blocked by local somatic application of TTX, other processes must also contribute. One likely additional mechanism is through the effect of somatic depolarization to increase the total number of dendritic spikes elicited by the synaptic pairing protocol, as we find that ITDP depends on the number of dendritic spikes. Finally, somatic depolarization is also likely to enhance ITDP by enhancing dendritic spike propagation, regardless of the increase in number of dendritic spikes. This conclusion is supported by our finding that when the resting membrane was depolarized a given number of dendritic spikes led to an increased onset of ITDP compared with when the membrane was at its normal negative resting potential. All the above factors likely combine to result in a greater depolarization at the proximal dendrites and soma to enhance the perisomatic $Ca^{2+}$ influx. Based on previous results, the enhanced $Ca^{2+}$ influx synergistically interacts with the activation of metabotropic glutamate receptors to trigger endocannabinoid release, which leads to the induction of ITDP (Dudman et al., 2007; Basu et al., 2013, 2016).

The effect of somatic depolarization to increase the probability of distal dendritic spike firing during the ITDP induction protocol is surprising, given that somatic depolarization produces only a small depolarization in the distal dendrite. Moreover, we find that this small distal depolarization is insufficient to alter the threshold of dendritic spiking in response to direct depolarizing current injection in the distal dendrite. One clue as to the potential mechanism for enhanced firing of dendritic spikes comes from our finding that the increase in the probability of dendritic spike firing during ITDP induction is not seen with the first few pairs of synaptic stimuli but only develops after several pairing events. This suggests that the pairing protocol gives rise to some form of activity-dependent intrinsic or synaptic plasticity process that enhances dendritic spiking, and that this plasticity mechanism is enhanced by somatic depolarization. Although further studies will be required to identify the basis of this plasticity, one simple hypothesis is that the plasticity itself is driven by dendritic spike firing, and that somatic depolarization enhances the plasticity by enhancing dendritic spike propagation to the soma.

Another potential mechanism by which somatic depolarization could, in principle, enhance dendritic spike propagation is through the enhancement of NMDA receptor opening and/or the firing of NMDA spikes. However, several lines of evidence suggest that enhanced NMDA receptor activation does not mediate the effect of somatic depolarization to enhance either dendritic spike propagation or ITDP induction. Thus, we found that DEDSP was observed even when a distal dendritic spike was directly triggered by dendritic current injection, and thus independent of NMDA receptor activation (Figs. 1, 2). Furthermore, we found that DEDSP occurred when only distal PP synapses were stimulated (Fig. 4). As somatic depolarization produced little change in resting potential in the distal dendrites, the sole site of NMDA receptor activation in these conditions, enhanced NMDA receptor activation is unlikely to account for enhanced dendritic spike propagation. Finally, a recent study investigating passive signal propagation in CA1 PN dendrites found that blocking NMDA receptors has only marginal effects on the somatic voltage-dependent amplification of single EPSPs or trains of EPSP (Hsu et al., 2018).

Although we cannot directly test whether the effect of somatic depolarization to enhance ITDP results from enhanced NMDA receptor activation at the SC synapses, because NMDA receptors are required for the induction of ITDP (Dudman et al., 2007), we also think it unlikely for the following reasons. First, the depolarization in the proximal dendrite in response to a 15-mV somatic depolarization is small (<5–10 mV), and much less than the 70- to 100-mV depolarization typically required to induce classic NMDA receptor-dependent plasticity (Chen et al., 1999). Second, somatic depolarization paired with a SC-evoked EPSP alone (without a dendritic spike) failed to induce plasticity under the conditions of our experiment, suggesting minimal $Ca^{2+}$ influx or plasticity in the absence of a dendritic spike. Finally, our finding that closed loop blockade of dendritic spikes with subthreshold EPSPs left intact was sufficient to suppress ITDP suggests that $Ca^{2+}$ influx via NMDA receptors alone is insufficient to induce plasticity.

In addition to ITDP, we speculate that other NMDA receptor-dependent forms of plasticity that require coordinated activity in multiple subcellular compartments may also be enhanced as the soma is depolarized. STDP is one such example, where dendritic excitability in conjunction with bAPs promotes synaptic plasticity (Bi and Poo, 1998; Kampa et al., 2006). Given that both dendritic excitability and back-propagation of sodium spikes are modulated by membrane potential, a more depolarized cell may generate a more efficient STDP, potentially with a longer time window for plasticity to occur. Furthermore, the additional somatic depolarization that DEDSP provides may in turn cause additional somatic APs (as seen in Fig. 5), which have an impact on plasticity mechanisms as well. Another form of plasticity involving dendritic spikes is the recently discovered behavioral time scale plasticity or BTSP (Bittner et al., 2017). In this form of plasticity, a dendritic plateau potential and the resulting complex spikes produce a long-term enhancement of EPSPs that occur over a seconds-long time window preceding the dendritic spike. While the exact intracellular mechanisms and synaptic inputs generating this form of plasticity are as yet unclear, it is likely that a gating mechanism such as DEDSP may well serve a modulatory role to promote this form of plasticity. Given the very different time scales and synaptic learning rules between BTSP and ITDP, further studies will be required to elucidate whether and how these forms of plasticity may be linked.

As many factors contribute to determining the somatic membrane potential, our results have a number of additional implications. First, what was formerly perceived as subthreshold background activity in neurons *in vivo* can, by influencing resting potential, powerfully regulate a neuron's spiking output and tune its sensitivity toward plasticity. This will serve to increase a neuron's computational capability at the subthreshold level as a given input, even if it does not contribute to a spike directly, will be able to modulate neural responsiveness throughout a neuron's complex dendritic arbor, even to events that arise in a different subcellular compartment. Such a mechanism, for example, would allow subthreshold input at a neuron's basal dendrites to enhance spike propagation of distal inputs along the apical dendrite. Second, as neuromodulatory

transmitters often act to regulate resting potential, DEDSP may also contribute to effects of arousal and attention on memory storage and sensory perception. Future *in vivo* studies will be of interest to examine how dendritic spike propagation is regulated during relevant behaviors and how direct manipulations of dendritic spike propagation efficacy may alter those behaviors.

## References


Alle H, Geiger JR (2006) Combined analog and action potential coding in hippocampal mossy fibers. Science 311:1290–1293.

Amitai Y, Friedman A, Connors BW, Gutnick MJ (1993) Regenerative activity in apical dendrites of pyramidal cells in neocortex. Cereb Cortex 3:26–38.

Bar-Yehuda D, Korngreen A (2008) Space-clamp problems when voltage clamping neurons expressing voltage-gated conductances. J Neurophysiol 99:1127–1136.

Basu J, Srinivas KV, Cheung SK, Taniguchi H, Huang ZJ, Siegelbaum SA (2013) A cortico-hippocampal learning rule shapes inhibitory microcircuit activity to enhance hippocampal information flow. Neuron 79:1208–1221.

Basu J, Zaremba JD, Cheung SK, Hitti FL, Zemelman BV, Losonczy A, Siegelbaum SA (2016) Gating of hippocampal activity, plasticity, and memory by entorhinal cortex long-range inhibition. Science 351:aaa5694.

Bi GQ, Poo MM (1998) Synaptic modifications in cultured hippocampal neurons: dependence on spike timing, synaptic strength, and postsynaptic cell type. J Neurosci 18:10464–10472.

Bittner KC, Grienberger C, Vaidya SP, Milstein AD, Macklin JJ, Suh J, Tonegawa S, Magee JC (2015) Conjunctive input processing drives feature selectivity in hippocampal CA1 neurons. Nat Neurosci 18:1133–1142.

Bittner KC, Milstein AD, Grienberger C, Romani S, Magee JC (2017) Behavioral time scale synaptic plasticity underlies CA1 place fields. Science 357:1033–1036.

Brun VH, Otnass MK, Molden S, Steffenach HA, Witter MP, Moser MB, Moser EI (2002) Place cells and place recognition maintained by direct entorhinal-hippocampal circuitry. Science 296:2243–2246.

Brun VH, Leutgeb S, Wu HQ, Schwarcz R, Witter MP, Moser EI, Moser MB (2008) Impaired spatial representation in CA1 after lesion of direct input from entorhinal cortex. Neuron 57:290–302.

Brunner J, Szabadics J (2016) Analogue modulation of back-propagating action potentials enables dendritic hybrid signalling. Nat Commun 7:13033.

Cai X, Liang CW, Muralidharan S, Muralidharan S, Kao JPY, Tang C-M, Thompson SM (2004) Unique roles of SK and Kv4.2 potassium channels in dendritic integration. Neuron 44:351–364.

Castle NA, Fadous S, Logothetis DE, Wang GK (1994) Aminopyridine block of Kv1.1 potassium channels expressed in mammalian cells and Xenopus oocytes. Mol Pharmacol 45:1242–1252.

Chagot B, Escoubas P, Villegas E, Bernard C, Ferrat G, Corzo G, Lazdunski M, Darbon H (2004) Solution structure of Phrixotoxin 1, a specific peptide inhibitor of Kv4 potassium channels from the venom of the theraphosid spider *Phrixotrichus auratus*. Protein Sci 13:1197–1208.

Chen HX, Otmakhov N, Lisman J (1999) Requirements for LTP induction by pairing in hippocampal CA1 pyramidal cells. J Neurophysiol 82:526–532.

Destexhe A, Babloyantz A, Sejnowski TJ (1993) Ionic mechanisms for intrinsic slow oscillations in thalamic relay neurons. Biophys J 65:1538–1552.

Diochot S, Drici MD, Moinier D, Fink M, Lazdunski M (1999) Effects of phrixotoxins on the Kv4 family of potassium channels and implications for the role of Ito1 in cardiac electrogenesis. Br J Pharmacol 126:251–263.

Dudman JT, Tsay D, Siegelbaum SA (2007) A role for synaptic inputs at distal dendrites: instructive signals for hippocampal long-term plasticity. Neuron 56:866–879.

Epsztein J, Brecht M, Lee AK (2011) Intracellular determinants of hippocampal CA1 place and silent cell activity in a novel environment. Neuron 70:109–120.

Gasparini S, Migliore M, Magee JC (2004) On the initiation and propagation of dendritic spikes in CA1 pyramidal neurons. J Neurosci 24:11046–11056.

Gasparini S, Losonczy A, Chen X, Johnston D, Magee JC (2007) Associative pairing enhances action potential back-propagation in radial oblique branches of CA1 pyramidal neurons. J Physiol 580:787–800.

Golding NL, Spruston N (1998) Dendritic sodium spikes are variable triggers of axonal action potentials in hippocampal CA1 pyramidal neurons. Neuron 21:1189–1200.

Golding NL, Jung HY, Mickus T, Spruston N (1999) Dendritic calcium spike initiation and repolarization are controlled by distinct potassium channel subtypes in CA1 pyramidal neurons. J Neurosci 19:8789–8798.

Golding NL, Staff NP, Spruston N (2002) Dendritic spikes as a mechanism for cooperative long-term potentiation. Nature 418:326–331.

Golding NL, Mickus TJ, Katz Y, Kath WL, Spruston N (2005) Factors mediating powerful voltage attenuation along CA1 pyramidal neuron dendrites. J Physiol 568:69–82.

Grienberger C, Chen X, Konnerth A (2014) NMDA receptor-dependent multidendrite Ca(2+) spikes required for hippocampal burst firing in vivo. Neuron 81:1274–1281.

Harvey CD, Collman F, Dombeck DA, Tank DW (2009) Intracellular dynamics of hippocampal place cells during virtual navigation. Nature 461:941–946.

Hines ML, Carnevale NT (1997) The NEURON simulation environment. Neural Comput 9:1179–1209.

Hoffman DA, Johnston D (1999) Neuromodulation of dendritic action potentials. J Neurophysiol 81:408–411.

Hoffman DA, Magee JC, Colbert CM, Johnston D (1997) K+ channel regulation of signal propagation in dendrites of hippocampal pyramidal neurons. Nature 387:869–875.

Hsu CL, Zhao X, Milstein AD, Spruston N (2018) Persistent sodium current mediates the steep voltage dependence of spatial coding in hippocampal pyramidal neurons. Neuron 99:147–162.e8.

Hulse BK, Moreaux LC, Lubenov EV, Siapas AG (2016) Membrane potential dynamics of CA1 pyramidal neurons during hippocampal ripples in awake mice. Neuron 89:800–813.

Iftinca M, McKay BE, Snutch TP, McRory JE, Turner RW, Zamponi GW (2006) Temperature dependence of T-type calcium channel gating. Neuroscience 142:1031–1042.

Jarsky T, Roxin A, Kath WL, Spruston N (2005) Conditional dendritic spike propagation following distal synaptic activation of hippocampal CA1 pyramidal neurons. Nat Neurosci 8:1667–1676.

Kaifosh P, Losonczy A (2016) Mnemonic functions for nonlinear dendritic integration in hippocampal pyramidal circuits. Neuron 90:622–634.

Kajiwara R, Wouterlood FG, Sah A, Boekel AJ, Baks-te Bulte LT, Witter MP (2008) Convergence of entorhinal and CA3 inputs onto pyramidal neurons and interneurons in hippocampal area CA1–an anatomical study in the rat. Hippocampus 18:266–280.

Kampa BM, Letzkus JJ, Stuart GJ (2006) Requirement of dendritic calcium spikes for induction of spike-timing-dependent synaptic plasticity. J Physiol 574:283–290.

Kerti K, Lorincz A, Nusser Z (2012) Unique somato-dendritic distribution pattern of Kv4.2 channels on hippocampal CA1 pyramidal cells. Eur J Neurosci 35:66–75.

Kim HG, Connors BW (1993) Apical dendrites of the neocortex: correlation between sodium- and calcium-dependent spiking and pyramidal cell morphology. J Neurosci 13:5301–5311.

Kim J, Jung SC, Clemens AM, Petralia RS, Hoffman DA (2007) Regulation of dendritic excitability by activity-dependent trafficking of the A-type K+ channel subunit Kv4.2 in hippocampal neurons. Neuron 54:933–947.

Larkum M (2013) A cellular mechanism for cortical associations: an organizing principle for the cerebral cortex. Trends Neurosci 36:141–151.

Larkum ME, Zhu JJ, Sakmann B (1999) A new cellular mechanism for coupling inputs arriving at different cortical layers. Nature 398:338–341.

Lee D, Lin BJ, Lee AK (2012) Hippocampal place fields emerge upon single-cell manipulation of excitability during behavior. Science 337:849–853.

Magee JC (1998) Dendritic hyperpolarization-activated currents modify the integrative properties of hippocampal CA1 pyramidal neurons. J Neurosci 18:7613–7624.

Magee JC, Carruth M (1999) Dendritic voltage-gated ion channels regulate the action potential firing mode of hippocampal CA1 pyramidal neurons. J Neurophysiol 82:1895–1901.

Maletic-Savatic M, Lenn NJ, Trimmer JS (1995) Differential spatiotemporal expression of K+ channel polypeptides in rat hippocampal neurons developing in situ and in vitro. J Neurosci 15:3840–3851.

Manita S, Miyakawa H, Kitamura K, Murayama M (2017) Dendritic spikes in sensory perception. Front Cell Neurosci 11:29.
Mehta MR (2004) Cooperative LTP can map memory sequences on dendritic branches. Trends Neurosci 27:69–72.
Mehta MR, Quirk MC, Wilson MA (2000) Experience-dependent asymmetric shape of hippocampal receptive fields. Neuron 25:707–715.
Migliore M (2003) On the integration of subthreshold inputs from perforant path and Schaffer collaterals in hippocampal CA1 pyramidal neurons. J Comput Neurosci 14:185–192.
Migliore M, Hoffman DA, Magee JC, Johnston D (1999) Role of an A-type K+ conductance in the back-propagation of action potentials in the dendrites of hippocampal pyramidal neurons. J Comput Neurosci 7:5–15.
Moczydlowski E, Latorre R (1983) Gating kinetics of Ca2+-activated K+ channels from rat muscle incorporated into planar lipid bilayers. Evidence for two voltage-dependent Ca2+ binding reactions. J Gen Physiol 82:511–542.
Nakashiba T, Young JZ, McHugh TJ, Buhl DL, Tonegawa S (2008) Transgenic inhibition of synaptic transmission reveals role of CA3 output in hippocampal learning. Science 319:1260–1264.
Neumaier F, Alpdogan S, Hescheler J, Schneider T (2020) Zn2+-induced changes in Cav2.3 channel function: an electrophysiological and modeling study. J Gen Physiol 152:e202012585.
Palani D, Baginskas A, Raastad M (2010) Bursts and hyperexcitability in non-myelinated axons of the rat hippocampus. Neuroscience 167:1004–1013.
Poirazi P, Brannon T, Mel BW (2003) Arithmetic of subthreshold synaptic summation in a model CA1 pyramidal cell. Neuron 37:977–987.
Ramakers GM, Storm JF (2002) A postsynaptic transient K(+) current modulated by arachidonic acid regulates synaptic integration and threshold for LTP induction in hippocampal pyramidal cells. Proc Natl Acad Sci U S A 99:10144–10149.
Santoro B, Grant SG, Bartsch D, Kandel ER (1997) Interactive cloning with the SH3 domain of N-src identifies a new brain specific ion channel protein, with homology to EAG and cyclic nucleotide-gated channels. Proc Natl Acad Sci U S A 94:14815–14820.
Schiller J, Schiller Y, Stuart G, Sakmann B (1997) Calcium action potentials restricted to distal apical dendrites of rat neocortical pyramidal neurons. J Physiol 505:605–616.
Stuart GJ, Spruston N (2015) Dendritic integration: 60 years of progress. Nat Neurosci 18:1713–1721.
Suh J, Rivest AJ, Nakashiba T, Tominaga T, Tonegawa S (2011) Entorhinal cortex layer III input to the hippocampus is crucial for temporal association memory. Science 334:1415–1420.
Sun Q, Srinivas KV, Sotayo A, Siegelbaum SA (2014) Dendritic Na+ spikes enable cortical input to drive action potential output from hippocampal CA2 pyramidal neurons. Elife 3:e04551.
Suter BA, O'Connor T, Iyer V, Petreanu LT, Hooks BM, Kiritani T, Svoboda K, Shepherd GM (2010) Ephus: multipurpose data acquisition software for neuroscience experiments. Front Neural Circuits 4:100.
Takahashi H, Magee JC (2009) Pathway interactions and synaptic plasticity in the dendritic tuft regions of CA1 pyramidal neurons. Neuron 62:102–111.
Takahashi N, Oertner TG, Hegemann P, Larkum ME (2016) Active cortical dendrites modulate perception. Science 354:1587–1590.
Waters J, Helmchen F (2004) Boosting of action potential backpropagation by neocortical network activity in vivo. J Neurosci 24:11127–11136.
Zhao X, Hsu CL, Spruston N (2022) Rapid synaptic plasticity contributes to a learned conjunctive code of position and choice-related information in the hippocampus. Neuron 110:96–108.e4.